iScience

CellPress
OPEN ACCESS

Article

Diffusion-limited cytokine signaling in T cell populations

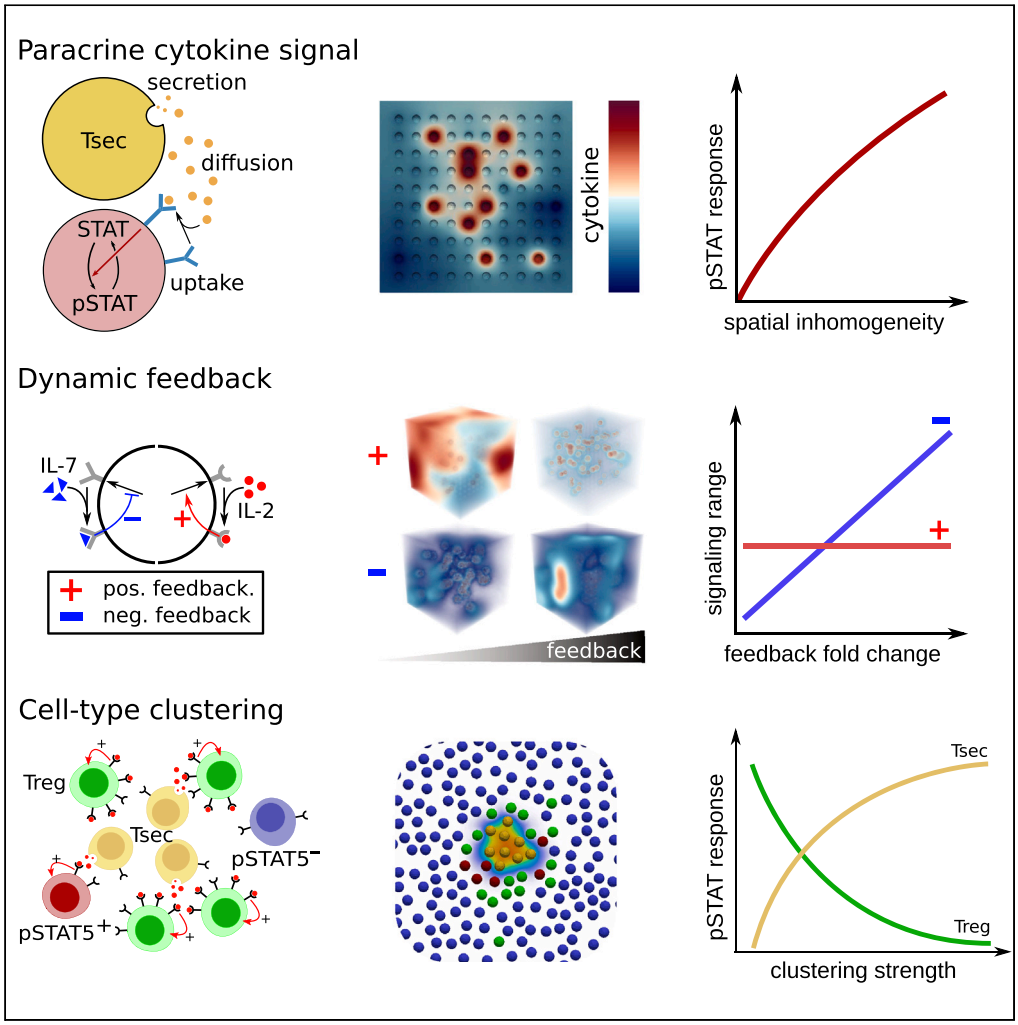

Patrick Brunner, Lukas Kiwitz, Lisa Li, Kevin Thurley

kevin.thurley@uni-bonn.de

Highlights

3D simulation framework to study immune-cell communication with diffusible ligands

Spatial concentration inhomogeneities amplify paracrine signaling strength

Quantitative characterization of the spatial cytokine niche and the signaling range

Co-clustering of T_{reg} cells with cytokine secreting cells effectively constrains signaling strength

Brunner et al., iScience 27, 110134
June 21, 2024
https://doi.org/10.1016/j.isci.2024.110134

iScience

CellPress
OPEN ACCESS

Article

Diffusion-limited cytokine signaling in T cell populations

Patrick Brunner,[1,2,3] Lukas Kiwitz,[1,2,3] Lisa Li,[1] and Kevin Thurley[1,2,4,*]

SUMMARY

Effective immune-cell responses depend on collective decision-making mediated by diffusible intercellular signaling proteins called cytokines. Here, we designed a three-dimensional spatiotemporal modeling framework and a precise finite-element simulation setup to systematically investigate the origin and consequences of spatially inhomogeneous cytokine distributions in lymph nodes. We found that such inhomogeneities are critical for effective paracrine signaling, and they do not arise by diffusion and uptake alone, but rather depend on properties of the cell population such as an all-or-none behavior of cytokine secreting cells. Furthermore, we assessed the regulatory properties of negative and positive feedback in combination with diffusion-limited signaling dynamics, and we derived statistical quantities to characterize the spatiotemporal signaling landscape in the context of specific tissue architectures. Overall, our simulations highlight the complex spatiotemporal dynamics imposed by cell-cell signaling with diffusible ligands, which entails a large potential for fine-tuned biological control especially if combined with feedback mechanisms.

INTRODUCTION

Interactions between immune cells play a fundamental role in the mammalian defense against pathogens. Specifically, the fine-tuned decision-making processes in the adaptive immune response comprise cell-cell communication among antigen-presenting cells (APCs) and T and B lymphocytes, employing surface-mediated signaling as well as diffusible ligands called cytokines.[1,2] Remarkably, different cytokine species may share important parts of the signaling machinery, including subunits of the high-affinity cytokine receptor as well as downstream signaling mediators, and still evoke different biological functions and regulatory properties. For instance, the cytokines interleukin (IL)-2 and IL-7 share the common gamma-chain of their receptors, and they both utilize STAT5 as major signaling mediator.[3] While IL-2 plays an essential role in the regulation of T cell activation as well as clonal expansion, IL-7 controls the homeostatic T cell population size. Furthermore, IL-2 signaling causes an increased expression of the high-affinity IL-2 receptor (IL-2R) on target cells,[4] while IL-7 signaling causes downregulation of IL-7 receptor (IL-7R) expression in T cells.[5] Due to its promoting effect on T cells, low-dose IL-2 therapy has been successfully employed in cancer immunotherapy and for autoimmune diseases, while IL-7 is utilized in the treatment of infectious diseases.[6–9]

In the case of paracrine cytokine signaling, the cytokine sources and sinks are often separated,[10] which may result in a spatially uneven cytokine concentration due to consequences of diffusive cytokine transport.[11] Indeed, previous model simulations have predicted spatial inhomogeneities in cytokine concentration spanning several orders of magnitude, within a physiological parameter regime.[12–14] Those results have been supported by experimental findings of notable and tunable inhomogeneities of the cytokine concentration in lymph nodes, which regulate the formation of local cytokine micro-environments.[15–18] Nevertheless, the measured fast diffusion coefficients for cytokines such as IL-2 may counteract the effects of localized cytokine secretion and uptake,[17,19] suggesting a subtle balance of several regulatory mechanisms controlling the spatial distribution and signaling range of cytokines. In fact, theoretical as well as experimental studies have indicated that spatial cytokine inhomogeneities can be fine-tuned by properties of the cell population,[13,16,20] but the range and effect size of such mechanisms remains unclear. Furthermore, it is not known how different regulatory mechanisms employed by different cytokines, such as positive vs. negative feedback on receptor expression in the case of IL-2 and IL-7, specifically modulate their spatiotemporal signaling properties and how that relates to biological functions.

Next to the emergence and fine-tuned control of spatial cytokine inhomogeneities, a prevailing question concerns the consequences of cytokine inhomogeneities for paracrine signaling efficacy and, in more general terms, for decision-making processes of immune-cell populations. Intuitively, spatial cytokine inhomogeneities may promote signaling efficacy especially in the range of low average cytokine concentrations, because locally enriched concentrations in small microenvironments may act to overcome the threshold for signal induction at least in those areas. However, cytokine signaling processes are subject to complex inter- and intracellular non-linear dynamics as well as constraints

[1]Biomathematics Division, Institute of Experimental Oncology, University Hospital Bonn, Bonn, Germany
[2]Systems Biology of Inflammation, German Rheumatism Research Center (DRFZ), a Leibniz-Institute, Berlin, Germany
[3]Institute of Biology, Humboldt University, Berlin, Germany
[4]Lead contact
*Correspondence: kevin.thurley@uni-bonn.de
https://doi.org/10.1016/j.isci.2024.110134

imposed by the detailed tissue architecture. All those properties act together in shaping the spatiotemporal dynamics, and therefore have to be considered in a quantitative analysis of the spreading and efficacy of paracrine cytokine signals.

Here, we designed a precise yet flexible three-dimensional mathematical simulation platform based on the finite-element method, to systematically analyze the interplay of tunable regulatory properties of paracrine cytokine signal propagation. Our investigation revealed the number of cytokine secreting cells as the primary driver of inhomogeneities in the cytokine field. Furthermore, feedback mechanisms involving receptor expression for both IL-2 and IL-7 regulate the activation of cells around a cytokine source, which we quantified in the model simulations by developing specifically tailored summary statistics. Finally, as the model allows for a variety of cytokine dynamics and interacting cells, we explored the consequences of specific tissue architectures on cytokine distribution and signaling. Throughout those multiple levels of paracrine interaction, we found that the complex diffusion and uptake dynamics generate properties of signal propagation that are quite different from a well-mixed scenario ignoring spatial inhomogeneities that is studied in parallel.

RESULTS

Spatially inhomogeneous cytokine concentrations arise generically and can induce potent and fine-tuned paracrine signals

Effective paracrine cytokine signaling requires concentrations exceeding a threshold for signal reception at the target cell,[21] and therefore is in conflict with the low measured values for the average concentration of many cytokine species.[13,22] Diffusion-limited signaling is a plausible mechanism for effective paracrine signaling even under conditions of low tissue-level cytokine concentrations, because locally amplified concentrations in the vicinity of cytokine-secreting cells may allow to exceed the signaling threshold on the surface of nearby responder cells. Nevertheless, such a mechanism requires a subtle balance of the rates of cytokine secretion, cytokine uptake, and cytokine diffusion, supplemented by intracellular processes including signaling cascades and transcriptional regulation. Here, we designed a three-dimensional mathematical model in terms of a diffusion problem in the extracellular space with cytokine secretion and uptake at the cell surface (Figure 1A and STAR Methods—Method details: Mathematical models). Hereby, the cytokine secretion rate is assumed to be a cell-type dependent constant, and the rate of cytokine uptake depends on the number of receptors expressed on the cell surface and on the local cytokine concentration. We additionally considered intracellular signal transduction by means of a conceptual model, where the phosphorylation level of the signal transducer and activator of transcription (STAT) in responder cells indicates effective paracrine signaling.

To systematically assess the robustness and dynamic range of diffusion-limited cytokine signaling in the context of regulatory properties of a cell population, we developed a spatiotemporal simulation work-flow based on an accurate and efficient finite-element solver (STAR Methods—Method details: Software and simulations). Due to the large timescale separation between diffusion (seconds), intracellular signaling (minutes) and processes that require transcriptional regulation (hours), we decided to employ a quasi-stationary state assumption to the reaction-diffusion problem throughout. Since we were interested in the systematic analysis of local cell-cell interactions, special consideration was put into a modular, scalable, and parallelizable modeling environment (Figure S1A). For the chosen mesh configuration, computation time scaled linearly with mesh fidelity and number of cells (Figure S1B), and the simulation error was largely set by boundary effects (Figures S1C–S1E) and therefore decayed rapidly with the number of cells.

To set the stage, we initially studied direct paracrine signaling activities in an otherwise stationary cell population, in terms of the well-studied model system of IL-2 secretion and uptake by T helper cells in a scenario with randomly assigned cytokine secreting and responder cells. Model parameters were determined in line with experimentally measured quantities[4,12,13,19,23–25] (Table 1), to foster simulation results in the physiological parameter regime. Following previous work,[16] we accounted for saturation effects regarding cytokine binding and uptake by cytokine receptors using a Michaelis-Menten type of equation, which we found to be a direct consequence of a mechanistic model formulation (STAR Methods—Method details: Mathematical derivations, "Description of saturated uptake dynamics"). In line with experimental data,[14,25,26] we assumed a discrete all-or-none type of IL-2 secretion in cytokine-secreting cells (the impact of this assumption is studied in detail in the following). Our modeling setup resulted in a high degree of spatial patterning due to cytokine concentration gradients between secreting and responding cells, which were also reflected in the downstream STAT signal (Figure 1B). As anticipated, our simulations revealed appreciable paracrine signaling efficacy due to increased spatial cytokine inhomogeneity as quantified by the spatial standard deviation (SD) or the concentration gradient (Figures 1C and S2A) of cytokine levels across responder cells.

Quite remarkably, high paracrine signaling activity of up to 40% pSTAT+ cells (Figure 1C) occurred in a regime where such signaling was undetectable in an identically parameterized ordinary differential equation (ODE, "well-mixed") system that arises naturally from a fast-diffusion assumption (STAR Methods—Method details: Mathematical derivations, "Deriving the well-mixed model"). Moreover, diffusion-limited signaling generated an appreciable dynamic range with regard to regulation by the amount of cytokine secreting cells, while the system was limited to an all-or-none response in the well-mixed situation (Figure S2B). Due to local accumulations of cytokine concentration, paracrine signaling efficacy exhibited a strong correlation with an increase in spatial cytokine inhomogeneity (Figure 1D). Due to local saturation effects in the cellular cytokine uptake, an increased average cytokine concentration compared to the well-mixed system (Figures 1E and S2C) can lead to further amplification of paracrine signaling activity.

To characterize our model system in more detail, we performed a systematic parameter sensitivity analysis with respect to standard parameter values (Table 1). That analysis revealed strong effects on signaling efficacy and cytokine inhomogeneity by the receptor number and the half-saturation constant for cytokine uptake K_D in addition to the cytokine secretion rate and the fraction of secreting cells (Figures 1F,S2D, and S2E). Interestingly, the rates of diffusion and extracellular cytokine decay as well as the cell-to-cell distance have a minor effect on

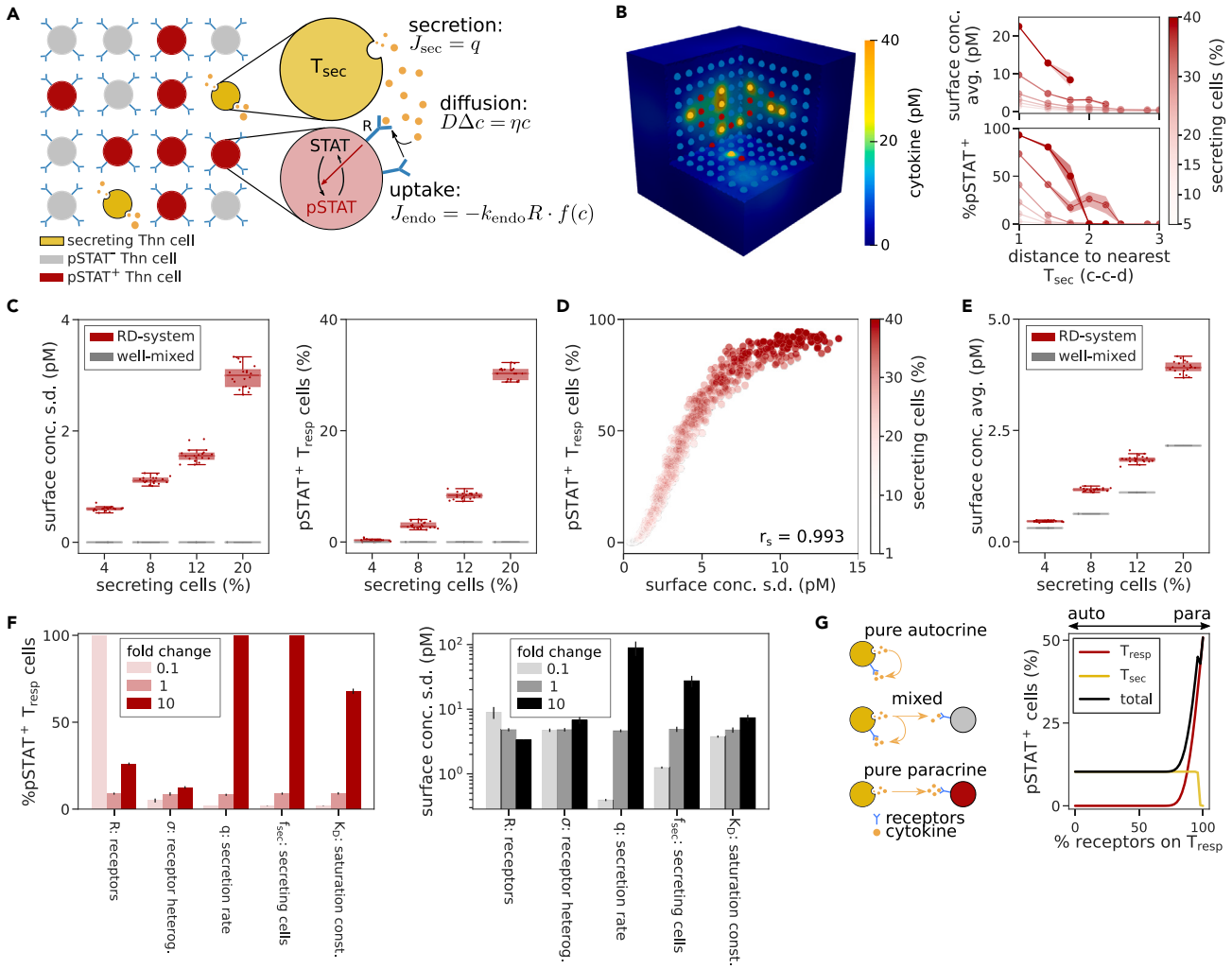

Figure 1. Spatial inhomogeneities induce stable paracrine signaling activity

(A) Model scheme. Cytokines are released by the secreting cells, and are subject to diffusion in the extracellular space and to binding to receptors on Thn cells. This binding and complex building is then translated into the phosphorylated STAT signal.

(B) Concentration profile. Typical model simulation using standard parameters (Table 1) and 5% secreting cells. Shown are the cytokine concentration field (left, see also legend in A) and the cytokine concentration and resulting pSTAT levels on responder cells (right). c-c-d, cell-to-cell distances. Maximum distance: 50% of average-distance between secreting cells.

(C) Model comparison. Spatial standard deviation (SD) of cytokine levels across responder cells and percentage of pSTAT+ cells for varying fractions of cytokine secreting cells, in the RD-system and corresponding well-mixed scenario, as indicated. Cells with pSTAT >0.5 are considered pSTAT+.

(D) Correlation analysis. Correlation between the fraction of pSTAT+ cells and the spatial standard deviation (SD) as shown in (C). Each dot represents a single simulation run. r_s is the Spearman's rank correlation coefficient.

(E) Cytokine concentration analysis. Average cytokine concentration on the cell surface across responding cells in the RD-system and corresponding well-mixed scenario, as indicated.

(F) Sensitivity analysis. The x axis indicates the parameter varied by a factor (fold-change) as indicated, all other parameters remain constant (cf. Table 1).

(G) Signaling mode. Scan from pure autocrine (all receptors on secreting cells) to pure paracrine (all receptors on responder cells) signaling as indicated by the cartoon. Shown is the percentage of pSTAT+ cells for responding cells (red), secreting cells (gold), or both (black).

Lines with shaded regions (B and C) and error bars (D and F) indicate averages and standard error of the mean (SEM) across 20 runs of the model simulation.

signaling efficacy and cytokine inhomogeneity. Hence, signaling amplification by diffusion-limited cytokine propagation is a generic mechanism that is robust to subtle changes in the spatial configuration of the system, but sensitive to properties that are under control of the participating immune-cell populations.

In line with that, experimental evidence[10] and theoretical considerations[19] suggest the ratio of receptors between secreting and responding cells to be a carefully controlled property that determines the mode of cytokine signaling in the range between purely autocrine and

Table 1. Standard parameter values

Parameter	Value	Unit	Description	Source
N_{cells}	1000		Amount of cells in the system	
d_c	20	µm	Shortest distance between cell centers	
r_c	10	µm	Cell radius	
D	10	$\mu m^2/s$	Diffusion coefficient	Höfer et al.[19]
I	10^{-12} - 10^{-9}	mol/l	Cytokine concentration range	Feinerman et al.[4]
f_{sec}	5	%	Fraction of secreting cells	
f_{resp}	95	%	Fraction of responder cells	
q	10	molecules/(cell *s)	Cytokine secretion rate	
R_{sec}	100	molecules/cell	Receptor count of secreting cells	
R_{resp}	10^4	molecules/cell	Receptor count of responder cells	
k_{on}	$3.1 * 10^7$	l/(mol *s)	Cytokine-receptor association rate	Wang and Smith[23]
H	$2.8 * 10^{-5}$	1/s	Cytokine decay rate	Busse et al.[12]
σ	1		Receptor heterogeneity, SD of log-normal distribution	Feinerman et al.[4]
Saturation parameters				
k_{off}	$2.3 * 10^{-4}$	molecules/s	Receptor disassociation rate	Wang and Smith[23]
k_{endo}	$4.6 * 10^{-4}$	molecules/s	IL-2*R complex internalization rate	Wang and Smith[23]
K_D	$7.423 * 10^{-12}$	mol/l	Half-saturation constant cytokine concentration	k_{off}/k_{on}
Receptor feedback				
k_{base}	$1 * 10^{-3}$	molecules/s	Minimum receptor production rate	
ν	0.0014	molecules/s	Receptor decay rate	Busse et al.[12]
K_m	0.5		Half-saturation constant pSTAT5	
γ	0.1 or 10		Feedback fold-change negative or positive feedback	
pSTAT signaling				
K_{EC50}	860	molecules	Half-saturation constant EC50	Cotari et al.[24]
E_{max}	$125 * 10^{-12}$	mol/l	Maximum EC50	Feinerman et al.[4]
E_{min}	0	mol/l	Minimum EC50	Feinerman et al.[4]
N_{EC50}	0.55–1.5		Hill coefficient EC50	Feinerman et al.[4]
N_{pSTAT5}	3		Hill coefficient pSTAT5	Cotari et al.[24]
IL-2 specific simulations (Figures 3, 4, and 5)				
q_{sec}	10	molecules/(cell *s)	IL-2 secretion rate	Han et al.[25]
R_{sec}	100	molecules/cell	Receptor count of secreting cells	Feinerman et al.[4]
R_{resp}	1500	molecules/cell	Receptor count of responder cells	Feinerman et al.[4]; Cotari et al.[24]
IL-7 specific simulations (Figures 3, 4, and 5)				
q_{sec}	100	molecules/(cell *s)	IL-7 secretion rate	
R_{sec}	0	molecules/cell	Receptor count of secreting cells	
R_{resp}	$5 * 10^5$	molecules/cell	Receptor count of responder cells	

purely paracrine signaling (Figure 1G). In our simulations, we found that paracrine signaling is limited to situations with more than 75% of all cytokine receptors expressed on responder cells and a subsequent increase in spatial inhomogeneity (Figures 1G, S2F, and S2G). On the other hand, cytokine secreting cells require only a minimal amount of receptor expression to receive an appreciable cytokine signal. That discrepancy is in line with the requirement for careful control of paracrine inflammatory signals such as IL-2 in order to prevent a potentially lethal cytokine storm,[27,28] and may explain the previously observed[29] downregulation of the pSTAT5 signaling pathway in cytokine secreting cells.

Overall, we found that a diffusion-limited mode of cytokine signaling allows for effective paracrine signaling in a physiological parameter regime where such signaling would be ineffective in a comparable well-mixed scenario, due to the low average cytokine concentrations.

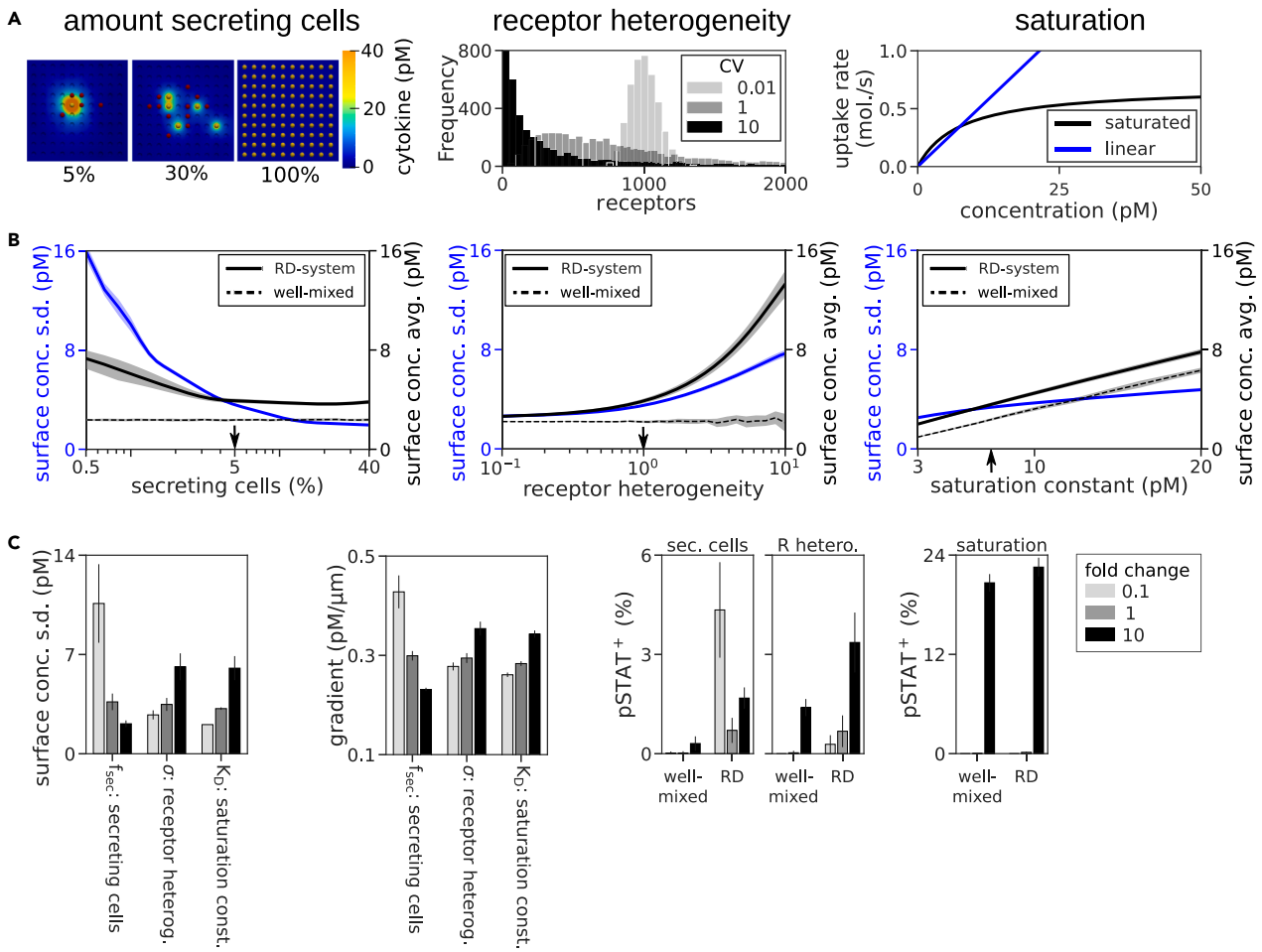

Figure 2. Systematic analysis reveals major drivers of cytokine inhomogeneity

(A and B) Sources of inhomogeneity. Analysis of cytokine inhomogeneity with respect to the fraction of cytokine secreting cells, receptor heterogeneity and saturation constant as indicated. In contrast to the analysis in Figure 1, simulations are designed in such a way that the total number of secreted cytokine molecules and the total number of cytokine receptors in the system are conserved through all simulations, see text for details. Shown are (A) a visualization and (B) a systematic scan for the parameter under study with respect to the spatial SD and spatial average (cf. Figure 1C), all other parameters are kept at standard values (Table 1). Vertical arrows indicate standard parameter values.

(C) Effect quantification. Sensitivity analysis of the parameters under study with respect to spatial SD, gradient and fraction of pSTAT+ cells, analogous to Figure 1F. Lines with shaded regions (B) and arrow (C) indicate average and standard error of the mean (SEM) across 20 runs.

Fractional abundance of cytokine secreting cells as major source of spatial inhomogeneity

Having established the generic occurrence and tunability of diffusion-limited paracrine signaling amplification, we sought to investigate the contributions of individual system components to cytokine concentration inhomogeneity. In our simulation, a uniform cell population, where cytokine secretion and uptake were equally distributed across cells, generated a nearly homogeneous cytokine concentration field, despite localized secretion and uptake at the cell surfaces (Figure 2A). Hence, we expected that a tight localization of cytokine sources is critical for spatial cytokine inhomogeneities, and we further sought to analyze the contributions of a heterogeneous distribution of cytokine receptors and of saturation effects in cytokine uptake dynamics on responder cells (Figure 2A). To this end, and to test the impact of an all-or-none-behavior of cytokine-secreting cells (that is few cells secreting large amounts of cytokine), we designed a simulation setup in which the total amount of secreted cytokine molecules and of cytokine receptor expression remain constant under parameter variation. We found that increasing the number of secreting cells in that system resulted in a steep decay of concentration inhomogeneities, approaching the well-mixed scenario (Figure 2B, left panel). The somewhat unexpected decay in the average cytokine concentration for low amounts of cytokine secreting cells (<5%) can be attributed to saturated uptake rates at high local concentrations. Indeed, that decay disappeared in the corresponding system with a linear uptake rate (Figure S3A and STAR Methods—Method details: Mathematical derivations, "Description of linear uptake dynamics"), in contrast to the decrease in spatial inhomogeneity that occurred also under linear uptake.

To account for cell-to-cell heterogeneity in cytokine receptor expression,[4,24,30] we considered expression values following a log-normal distribution at varying coefficients of variation, while keeping average expression levels constant (Figure 2A, middle panel). As anticipated, high levels of receptor heterogeneity induced appreciable cytokine inhomogeneities in the RD-system (Figure 2B, middle panel). Interestingly, in the RD-system, the average cytokine concentration also showed a substantial increase with receptor heterogeneity, although the total amounts of cytokine secretion and uptake were kept at a constant level so that cytokine concentrations remained unchanged in the well-mixed scenario. That seemingly paradoxical effect is independent of uptake-rate saturation (Figure S3B), and can be explained by the shape of a log-normal distribution, accounting for strong receptor heterogeneity resulting in few cells with very high uptake capacity and the remaining cells showing low uptake rates. In line with that, the observed increase of the average cytokine concentration could be analytically reconciled (Figure S3C) by the help of a previously established[13] approximate solution of the reaction-diffusion problem that is valid in the vicinity of cytokine secreting cells.

Finally, we considered the effects of varying the saturation constant in our system. Interestingly, substantial differences regarding average cytokine concentration values between linear and saturated uptake functions occurred only in parameter ranges with very high secretion rates (Figure S3D), which are reached at low fractions of cytokine-secreting cells (cf. caption to Figure 2B). In line with that, increased values of the saturation constant induced only moderately higher values of the spatial inhomogeneity, and a nearly proportional change in concentration (Figure 2B, right panel) (cf. STAR Methods—Method details: Mathematical derivations, "Description of linear uptake dynamics"), in both the reaction-diffusion and the well-mixed system.

Notably, across all three parameters under study, we found that any increase in inhomogeneity was accompanied by a similar rise in activation (Figures 2C, S3E, and S3F). While that increased signaling activity can be partially attributed to the increased average cytokine concentration in all three cases, the change in cytokine concentration values is lowest and the increase in spatial inhomogeneity is the highest in the case of a decrease in the fraction of cytokine secreting cells.

Hence, we conclude that the highly localized mode of cytokine secretion mediated by a small number of cytokine secreting cells is the main driver of cytokine inhomogeneities, and thus the all-or-none property that was frequently observed for cytokine secretion is critical for paracrine signaling efficacy.

Dynamic feedback on receptor expression modulates spatial cytokine gradients

In addition to the mere exchange of paracrine signals studied so far, immune-cell populations have been found to exhibit feedback regulation directly on the level of cell-cell communication, in terms of cytokine receptor expression levels depending on the local cytokine environment.[5,31–33] Therefore, we proceeded to study the impact of such feedback mechanisms on the cytokine concentration field. Since modulation of receptor expression levels requires transcriptional regulation, considering such processes introduces a new timescale on the order of hours to the system, giving rise to an intertwined combination of a quasi-stationary reaction-diffusion problem and a comparatively slow, dynamic modulation of cellular properties. In immune-cell compartments such as the lymph node, experiments have shown that several lymphocyte populations show high degrees of random and directed cell motility; in many cases achieving cell speeds on the same timescale (hours). However, upon effective antigen stimulation, T cells remain bound to an antigen-presenting cell via the immunological synapse until they reach their full activation status by means of additional cytokine signaling.[34,35] That gives rise to an immobilized population of antigen-exposed responder cells, which is the focus of our study.

Positive and negative feedback on cytokine receptor expression are widespread properties of immune-cell populations. To describe this behavior, we extended our original model (Figure 1A) by introducing a local cytokine concentration dependent receptor expression on responding cells, resulting in a time dependent model. We also introduced our established response-time modeling framework to the intracellular pSTAT5 transcription pathway[36,37] (Figure S4A). Here, we focused on two well-established examples, which are the IL-2/IL-2R system for positive feedback and the IL-7/IL-7R system for negative feedback (Figure 3A). In both cases, naive T helper cells act as responder cells. In the case of IL-2, cytokine secreting cells correspond to fully activated T cells under high antigen stimulation,[7] and in the contrasting scenario of IL-7 signaling, stromal cells take the role of secreting cells.[5,38]

In the IL-2 scenario, upon initializing cytokine secretion, the system quickly reached a transient state of high systemic cytokine concentration accompanied by increased STAT5 signaling activity and a subsequent increase in IL-2 receptor expression (Figures 3B and S4B–S4D, left panels), in agreement with experimental data.[30] To analyze the effects of negative feedback by means of the homeostatic IL-7 signal in comparison to positive feedback, we considered a thought experiment where the system is initially deprived of cytokine (Figures 3B and S4B–S4D, right panels). Upon initializing cytokine secretion, responding cells decreased receptor levels due to negative feedback, resulting in increased levels of cytokine concentration and STAT5 signaling. In the corresponding well-mixed simulations (Figures 3B and S4C), cytokine concentrations remained below threshold for signal induction in both the IL-2 and the IL-7 scenarios.

Next, we sought to analyze the properties of positive and negative feedback in more detail. Generally, the population of responding cells can be categorized into two groups: (1) cells capable of maintaining a high level of STAT5 signaling activity, and (2) cells that are unable to receive sufficient signal after an initial transient (Figures S4E–S4G). The emerging bimodal distribution for positive feedback is not present in well-mixed scenarios and shows a strong dependence on the feedback fold change (Figure 3C, left panel). On the other hand, negative feedback induced a more gradual response for both the well-mixed and RD-system, with the RD-system yielding a higher fraction of cells exhibiting stable STAT5 signaling activity (Figure 3C, right panel). Next to those differences regarding STAT5 distributions, also the time to activation shows marked differences between positive and negative feedback regulation (Figure 3D), with negative feedback showing a much slower response time that is subject to modulation by feedback fold change. Quite interestingly, strong positive feedback

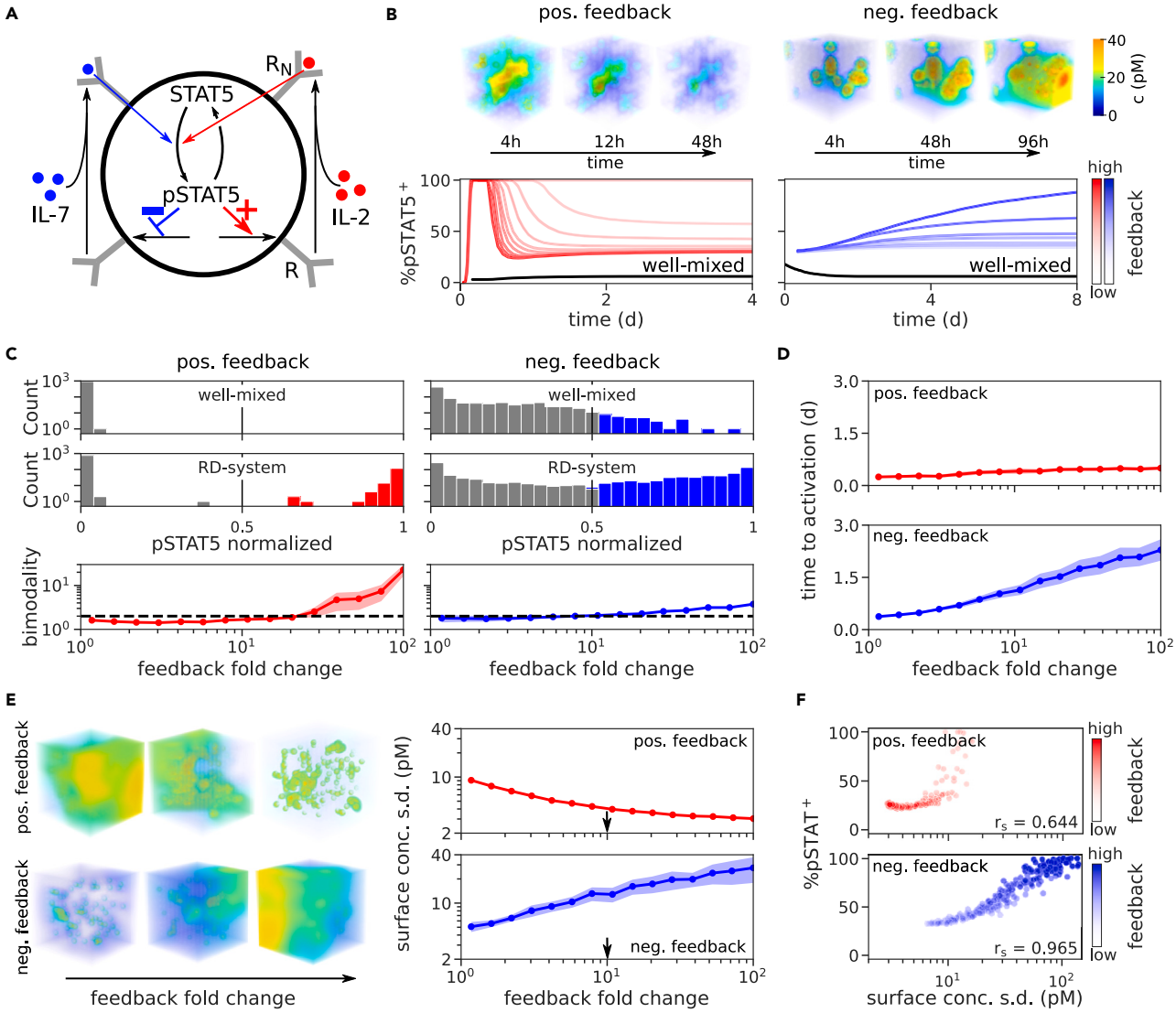

Figure 3. Feedback on receptor expression generates complex spatiotemporal dynamics

(A) Introducing feedback. Model scheme for positive and negative feedback on cytokine receptor expression. The pSTAT signal downstream of paracrine cytokine signaling induces either an increase (positive feedback, "IL-2") or a reduction (negative feedback, "IL-7") of receptor expression.

(B) Kinetic feedback response. Kinetic simulation of the model illustrated in (A), see text for details. Shown are the cytokine concentration field at three different time points (top), and the paracrine signaling efficacy measured by fraction of pSTAT5+ cells at varying feedback fold change γ (bottom).

(C) Bimodality analysis. Cytokine receptor expression for positive and negative feedback. Shown are histograms of the pSTAT5 signal across cells (top), and the resulting bimodality as measured by Ashman's D (bottom), at the last time point. Gray bars represent cells falling below a threshold value of 0.5 for pSTAT5, and dashed lines indicate a threshold value of 2 for Ashman's D indicating significant bimodality.

(D) Response time. Time until cells that are pSTAT5+ at steady-state (cf. C) reach the threshold value of 0.5 for the first time.

(E) Influence on inhomogeneity. Analysis of spatial cytokine inhomogeneity with respect to receptor feedback. Shown are cytokine concentration fields (left) and corresponding values of the spatial SD in dependence of the feedback fold change γ (right), for positive and negative feedback as indicated. Vertical arrows indicate standard parameter values.

(F) Correlation analysis. Correlation between the fraction of $pSTAT^+$ cells and the spatial SD depending on feedback fold change. Each dot represents a single run. r_s is the computed Spearman's rank correlation coefficient.

Lines with shaded regions (C and E) represent average and SEM across 20 runs of a simulation.

induced a decay and strong negative feedback induced an increase in measures of spatial cytokine inhomogeneity (Figures 3E, S4H, and S4I), due to opposed effects on signal localization. This change in signal localization results in a similar change in cytokine signaling efficacy (Figure 3F), which is in line with the notion of the IL-7 receptor as an "altruistic" signaling mediator,[39] as IL-7 uptake is stopped upon signal reception, so that cells further away from the cytokine-secreting cell are able to receive cytokine molecules.

In conclusion, we found the introduction of dynamic feedback on cytokine receptor expression to be an important control mechanism for the distribution and timing of cytokine concentrations, and hence also for paracrine signaling efficacy.

Regulatory properties of the cytokine signaling niche

To understand the intertwined regulation of paracrine signaling via spatial inhomogeneities and feedback regulation in more detail, we shifted our focus to the immediate neighborhood of each secreting cell, which has previously been referred to as signaling niche.[16] Based on the results on feedback-driven spatial inhomogeneity (cf. Figure 3E), we hypothesized that positive feedback restricts the signaling range and negative feedback amplifies the signaling range, thus potentially enabling effective signaling toward a larger group of responder cells.

To identify the signaling niche of an individual cytokine secreting cell, we utilized density-based spatial clustering of applications with noise (DBSCAN) and defined a signaling niche as a cluster that contains at least one cytokine secreting cell and at least one activated cell (Figures 4A and 4B). Hence, the maximum possible number of niches equals the number of secreting cells (black line in Figure 4B), and since one cytokine-secreting cell is insufficient for effective paracrine signaling in the physiological parameter regime, the realized number of niches in the system typically falls far below that maximal number. Notably, we found that positive feedback leads to increased signaling activity inside a niche, and negative feedback to a higher fraction of activated cells outside the niche (Figure 4C), in line with our hypothesis on the signaling range.

To proceed to a more direct quantitative analysis, we defined the "niche score" as the ratio between the number of niches and the number of secreting cells, and the "niche effect" as the ratio between the average pSTAT5 signal inside and outside of the niche (Figures 4D, 4E, and S5A). A high niche score indicates well-separated niches, and a high niche effect indicates that the signal is primarily located within the niche compared to outside, in other words, it accounts for the leakiness of the cytokine niche. Furthermore, our definition of the signaling niche allowed to quantify the signaling range as average distance between cytokine-secreting cells and maximal-distance responder cells within a niche. The niche score and niche effect in conjunction with the signaling range (Figures 4E and 4F) revealed that positive feedback enhances niche separation (high niche score) and induces a highly localized signal within each niche (high niche effect with low signaling range), while negative feedback causes niches to merge (low niche score) and increases cytokine leakiness (low niche effect and high signaling range).

Those system properties further depend on the number of secreting cells, with small numbers limiting the effect of both positive and negative feedback, since only few responder cells are activated (Figures 4G and S5B), and high numbers additionally dampening the effect of negative feedback (Figures 4H and S5C). That latter effect can be attributed to larger niches requiring longer signaling ranges, reflecting the previously detected (cf. Figure 3D) increase in activation time under negative feedback.

Overall, our detailed quantitative analysis of the signaling niche revealed that local receptor expression feedback has a strong influence not only on signaling efficacy with regard to nearby cells, but also regarding signaling range and niche separation, facilitating an adaptive response to variable stimulus intensities.

The local tissue architecture provides an additional regulatory layer for spatiotemporal cytokine signals

Thus far, to systematically investigate the spatiotemporal dynamics, cells were placed randomly on a cubic grid in all simulations shown. To analyze the effect of additional constraints imposed by the local tissue architecture, we also designed a grid-free simulation setup allowing to induce clustering of specific cell types in a tightly controlled manner, by variation of the clustering strength φ. That clustering strength correlates well with the silhouette and Calinski-Harabasz scores, which are established metrics for clustering quality (Figure S5D). Such clustering of specific cell types is a wide-spread property of immune-cell populations and can be mediated by chemokine signals or also physical barriers, such as imposed by stromal cells in the lymph node.[40,41]

Here, we initially considered a situation where IL-2 secreting T cells accumulate in the vicinity of specific APCs presenting their cognate antigen (Figure 5A). As expected, such co-localization of cytokine-secreting cells imposes a substantial increase in paracrine signaling efficacy in our simulations, since locally enriched cytokine concentrations levels allow to overcome the activation threshold in nearby cells. For low-to-moderate numbers of cytokine-secreting cells, quantitative analysis confirmed that effect in terms of the number of activated cells, the niche effect defined previously (Figure 5B) and the signaling range, despite an overall reduction of IL-2 concentration levels (Figure S5E). Quite interestingly, at very high numbers of cytokine-secreting cells, co-localization can also have the opposite effect and induces a reduction in the number of activated cells (Figure 5B, inset), which can be explained by the isolating effect of nearby responding cells preventing long-range paracrine signaling. To provide immune tolerance and reduce the risk of immune-responses to self-antigen, paracrine IL-2 signaling is mitigated by regulatory T (Treg) cells that express large numbers of high-affinity IL-2 receptor and can act as strong cytokine sinks.[15,19,42] In particular, it has been suggested that Treg cells can effectively take up IL-2, because they are stimulated by cognate antigen presented by the same antigen-presenting cell as the corresponding effector T cells and thus are co-localized in the same spatial signaling niche[18,43] (Figure 5C, left panel). Indeed, we found that the inhibitory effect of Treg cells is rather limited if they are placed randomly, that is $\varphi = 0$ (Figures 5C and 5D). At least a partial co-localization of Treg cells with cytokine-secreting cells seems required for effective reduction of cytokine signal and signaling range (Figure S5F), and can induce almost complete signal inhibition already at a fraction of only 4% Treg cells in our simulations.

While IL-2 signaling in the local environment created by APCs facilitates fast and unambiguous decision-making on T cell activation, it has been argued that IL-7, a cytokine essential for T cell survival, should be distributed more widely within the system.[39] Our results on the spatiotemporal effects of negative feedback (cf. Figure 4E) supported that claim, as we observed an increase in paracrine signaling efficacy and spatial range. To investigate that phenomenon in a more specific scenario, we introduced co-localization of IL-7 secreting cells analogous

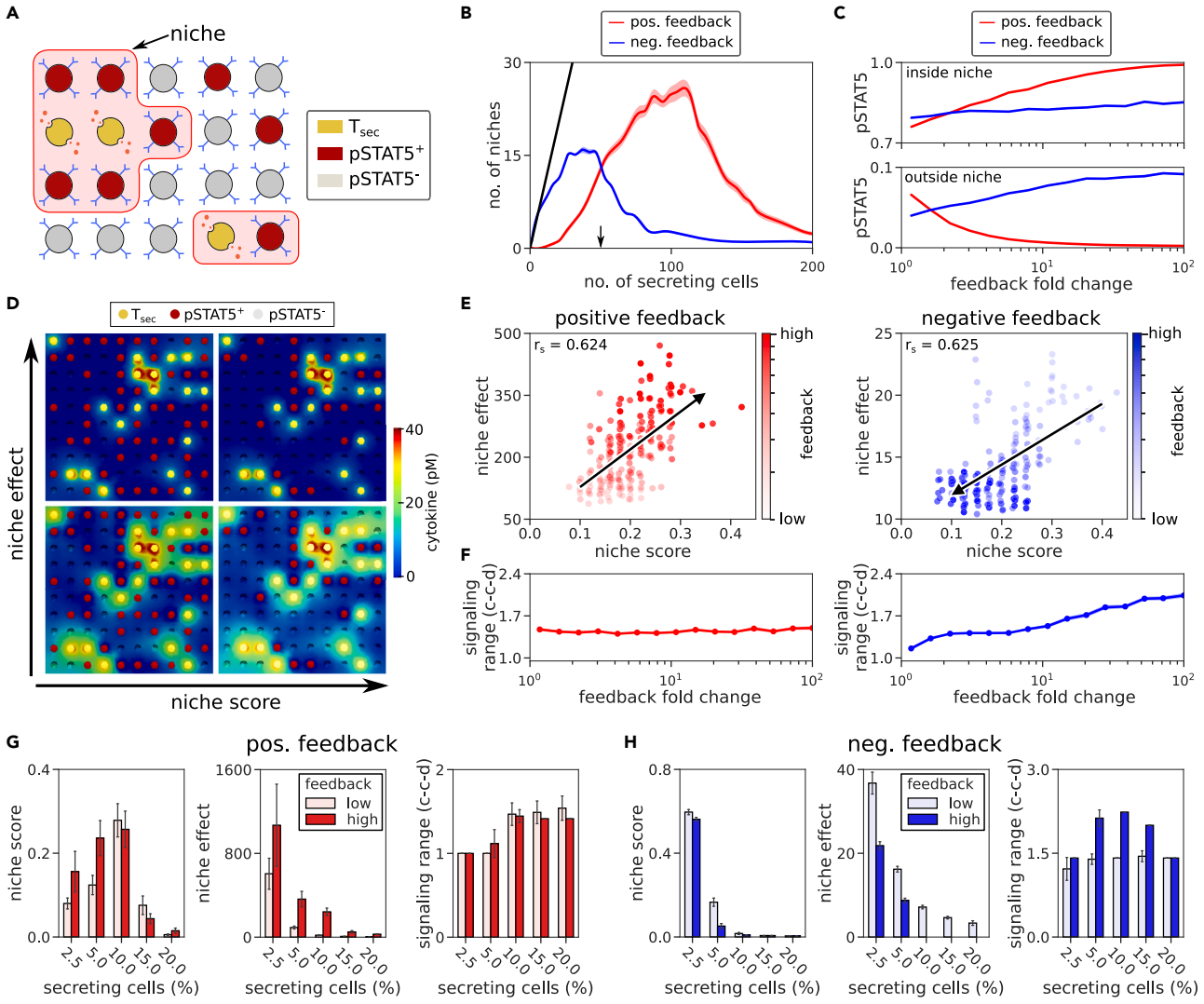

Figure 4. Niche score and niche effect characterize spatial patterning of paracrine cytokine signals

(A) Signaling niche. Schematic illustrating the definition of a cytokine signaling niche: upon clustering of cells by theirpSTAT5 values, a niche is defined as a cluster that contains at least one secreting cell and one pSTAT5+ cell.

(B) Niche quantification. Number of niches (cf. A) in dependence of the number of cytokine secreting cells. Black line: theoretical maximum (every T_{sec} cell forms a separate niche). Black arrow: standard parameter (cf. Table 1).

(C) Signal distribution. Average pSTAT5 values of cells inside and outside of a cytokine signaling niche.

(D) Niche derived metrics. Visualization of the quantities niche score and niche effect. For visualization purposes 15% secreting cells were used. The niche score is defined as the number of niches divided by the number of secreting cells in the system, the niche effect as the fraction of pSTAT5+ cells within the niche divided by outside of the niche. See also Figure S5A.

(E) Correlation analysis. Correlation between niche score and niche effect for positive and negative feedback. The black line shows a linear fit of all data points. The arrow head was added to indicate the direction of increased feedback. r_s is the computed Spearman's rank correlation coefficient.

(F) Signaling range in dependence of feedback fold change.

(G and H) Niche score, niche effect and signaling range for varying fractions of cytokine secreting cells. The bar color indicates feedback fold-change, low as $\gamma = 2$ and high as $\gamma = 100$, cf. (C) and (F).

Lines with shaded regions (B, C, and F) and error bars (F and G) indicate average and SEM across 20 runs of the simulation.

to the IL-2 case (Figure 5E). As anticipated, we found that increased clustering of cytokine-secreting cells not only improved signaling efficacy (Figures 5E and 5F), but also caused an increase in cytokine concentration levels and signaling range (Figure S5G).

Hence, we found that the spatial composition and especially local clustering of cell types can provide another layer of control over the range and efficacy of paracrine cytokine signaling, acting together with the amount of cytokine secreting cells, cytokine receptor expression and cytokine-dependent feedback regulation.

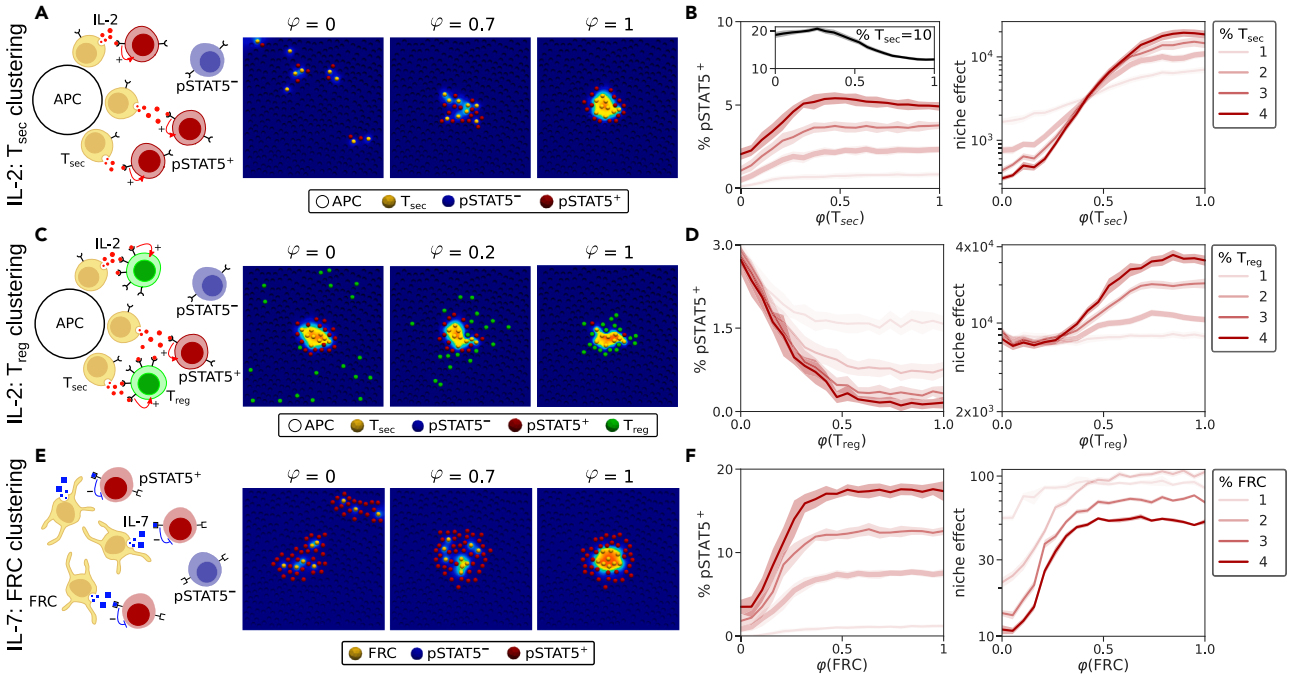

Figure 5. Spatiotemporal cytokine dynamics in the context of an established tissue architecture

(A) T_{sec} colocalization. Schematic (left panel) and typical simulations (right panel) of a scenario with IL-2 secreting T cells (T_{sec}) in the vicinity of an antigen-presenting cell (APC), surrounded by responder T cells. φ: clustering strength of T_{sec} cells. Shown are two-dimensional snapshots for the purpose of visualization, the analysis below is performed on full 3D-simulations.

(B) Clustering strength analysis. Analysis of the fraction of pSTAT5+ cells (left) and the niche effect (right) in dependence of the clustering strength φ for the scenario visualized in (A). Lines with shaded regions indicate average and SEM across 20 runs of each simulation.

(C and D) Treg colocalization. Regulatory T cells (T_{reg}) expressing high numbers of IL-2R are co-localized with T_{sec} cells in the vicinity of an antigen-presenting cell. See (A) and (B) above for details.

(E and F) Fibroblastic reticular cell (FRC) colocalization. FRCs secrete IL-7, which is taken up by naive T helper cells.

DISCUSSION

Cell-cell communication using diffusible ligands is a widespread mechanism to exchange information in multi-cellular organisms, and is particularly important in the collective decision-making processes of the mammalian immune system. Compared to intracellular processes, the larger spatial domain of such cell-cell interaction dynamics increases the potential for inhomogeneous distributions and non-intuitive spatial patterning[44,45] of signaling mediators. Nevertheless, the high diffusivity (~10 $\mu m^2/s$) of small proteins such as cytokines suggests that concentration inhomogeneities may disappear very rapidly on the relevant time- and length scales, that is cell-cell distances in lymph nodes (<5 μm) and times for signal integration and cell-differentiation (minutes to hours). By systematic analysis of physiological scenarios of cytokine signaling using an efficient finite-element simulation setup, we found that spatial cytokine inhomogeneities do not arise by diffusion processes per se. Rather, additional factors are required, such as a sparse occurrence and all-or-none behavior of cytokine secreting cells or heavily skewed distributions of cytokine receptors across cells. Thus, concentration inhomogeneities are essentially a property that is under control of the cell population.

Our mathematical formulation combines a description of signal processing on the cellular level with a biophysical description of cytokine diffusion, secretion, and uptake, leading to a quasi-stationary diffusion problem with non-linear Robin boundary condition. That description mandates a precise numerical solver, but requires fewer assumptions than a receptor mean field approach[16] or similar analytical formulations that could be derived under homogenization assumptions, i.e., replacing individual cells by a density of cells with negligible volumes.

The signaling range of cytokine-secreting cells is diffusion-limited, since cytokine uptake requires diffusion of the cytokine through extracellular space, in addition to binding to its high-affinity receptor.[46,47] The importance of this diffusion limit becomes apparent when considering the diminished signaling efficacy in our well-mixed model implementation. In the reaction-diffusion model, considering non-linear uptake dynamics on the surface of responding cells, we found that both the fraction of secreting cells and heterogeneity in receptor expression were able to generate cytokine concentration inhomogeneities. Previous studies have indicated values between 1% and 20% for the fraction of cytokine-secreting cells[14,25] and a coefficient of variation for the receptor distribution that is close to 1.[4,24] Under those conditions, our results suggest a higher contribution of the fraction of cytokine-secreting secreting cells to spatial inhomogeneities within the physiological parameter range.

Another important factor shaping cytokine signaling dynamics is feedback regulation of receptor expression on responding cells, which has been reported not only for IL-2 and IL-7 as the key interest of this study, but also for other cytokines including IL-4, IL-21, TGF-β, and

IFN-γ.[5,31–33,48–50] It is known that positive feedback can induce an all-or-none type of response to a signal, while negative feedback leads to more gradual and homogeneous dynamics and can have an effect on the timescale of the response to an input signal.[51,52] In line with that and with previous studies,[12] we found that spatial cytokine gradients can induce significant bifurcations in activation patterns of the naive T cell in the presence of positive feedback mediated by the cytokine IL-2. Interestingly, that model behavior does not occur in a parallel well-mixed scenario, highlighting the requirement of spatial cytokine distributions for paracrine stimulation even in the presence of positive feedback. Considering IL-7 as a cytokine promoting negative feedback on receptor expression, we observed an increase in signaling range that propagates with time, resembling a signaling wave that spreads through the cell population. That phenomenon is well in-line with the notion of IL-7 responder cells as "altruistic",[39] since they provide access to IL-7 to nearby cells by downregulating their receptors.

To quantify the localization and effectiveness of cytokine signaling within the microenvironment around cytokine-secreting cells, we propose the niche score and niche effect as summary statistics that may also serve for comparison with multi-color histology data in future research. The niche score offers an understanding of how well separated niches are, while the niche effect quantifies how effectively cytokine signal is localized within each niche. Utilizing these spatial statistics, we found that the upregulation of receptors in the IL-2 scenario results in a localization of activation and signal within a niche. We identified the opposite behavior in the case of IL-7 signaling, where downregulation of receptors delocalizes the signal, thus inducing a more homogeneous cytokine concentration field. Consequently, paracrine signaling efficacy depends more on the total amount of cytokine molecules in the system rather than its location, which is in line with the biological function of IL-7 as a survival signal controlling the size of a cell population in homeostasis.

Finally, we asked how the local tissue architecture in terms of already established clustering and co-localization of specific cell types would modulate signaling efficacy and spatial cytokine patterning. Our model simulations revealed that the spatial clustering of cytokine-secreting cells can substantially increase signaling efficacy, as cytokine secretion by multiple cells in a signaling niche combines to act on responder cells. Moreover, we found that co-localization of cytokine-secreting cells and cells with a high capacity of cytokine uptake, such as described for Treg cells in the context of IL-2 signaling,[18] is a highly efficient mechanism to control the effectivity of paracrine signals and thus modulate the degree of immune tolerance.

Overall, we found that the spatial relationships and individual properties of cytokine-secreting cells and cells expressing high-affinity cytokine receptor species can critically regulate the efficacy of cell-communication. Future research may combine our approach with quantitative models on germinal-center dynamics[53–55] and multiplexed histology data[56–58] characterizing tissue organization in lymphoid organs and the tumor micro-environment, paving the way to a unified, quantitative understanding of spatiotemporal decision-making in immune-cell populations.

Limitations of the study

Focusing on a systematic analysis of cytokine signaling in the context of IL-2 and IL-7, our setup does not fully capture the complex dynamics imposed by the diverse array of cytokines and cell types present in lymph nodes. In particular, while secreting cells attach to APCs and arrest their movement, responding cells do not exhibit the same behavior, so that it will be elucidating to incorporate directed and random cell motility into our simulation framework in future research. Additionally, while the biophysics of IL-2 is relatively well studied, and parameters such as diffusion and binding constants, receptor expression levels and secretion rate have been determined experimentally, the situation is different for IL-7, posing a challenge for parameter annotation in that case. Here, we extrapolated the STAT5 activation function from IL-2 to IL-7 as both cytokines share the gamma-chain of the high-affinity cytokine receptors, and they both utilize STAT5 as major signaling mediator. However, the necessity to integrate such assumptions underscores the need for a systematic quantification of cytokine signaling processes beyond IL-2.

STAR★METHODS

Detailed methods are provided in the online version of this paper and include the following:

- KEY RESOURCES TABLE
- RESOURCE AVAILABILITY
  - Lead contact
  - Materials availability
  - Data and code availability
- METHOD DETAILS
  - Mathematical models
  - Software and simulations
  - Mathematical derivations
- QUANTIFICATION AND STATISTICAL ANALYSIS
  - Statistics
  - Quantifying spatial patterns: Niche score, niche effect and signaling range

SUPPLEMENTAL INFORMATION

Supplemental information can be found online at https://doi.org/10.1016/j.isci.2024.110134.

ACKNOWLEDGMENTS

We thank Andreas Hutloff (University Hospital Kiel, Germany), Thomas Schüler (University Hospital Magdeburg, Germany), and members of the Thurley group for fruitful discussions. This work was supported by the Deutsche Forschungsgemeinschaft (TH 1861/5-1 and TH 1861/7-1), Germany's Excellence Strategy (EXC2151-390685813 and EXC2047-390873048), and the Leibniz Association, Germany (Best-minds junior research group), all to K.T.

AUTHOR CONTRIBUTIONS

Conceptualization, K.T.; methodology, software and visualization, P.B. and L.K.; formal analysis, P.B., L.L., and K.T.; writing – original draft, P.B., with input from all other authors; writing – review and editing, K.T.

DECLARATION OF INTERESTS

The authors declare no competing interests.

Received: January 5, 2024
Revised: March 30, 2024
Accepted: May 25, 2024
Published: May 30, 2024

REFERENCES

1. Lin, J.-X., and Leonard, W.J. (2019). Fine-Tuning Cytokine Signals. Annu. Rev. Immunol. *37*, 295–324. https://doi.org/10.1146/annurev-immunol-042718-041447.
2. Morel, P.A., Lee, R.E.C., and Faeder, J.R. (2017). Demystifying the cytokine network: Mathematical models point the way. Cytokine *98*, 115–123. https://doi.org/10.1016/j.cyto.2016.11.013.
3. Leonard, W.J., Lin, J.-X., and O'Shea, J.J. (2019). The γc Family of Cytokines: Basic Biology to Therapeutic Ramifications. Immunity *50*, 832–850. https://doi.org/10.1016/j.immuni.2019.03.028.
4. Feinerman, O., Jentsch, G., Tkach, K.E., Coward, J.W., Hathorn, M.M., Sneddon, M.W., Emonet, T., Smith, K.A., and Altan-Bonnet, G. (2010). Single-cell quantification of IL-2 response by effector and regulatory T cells reveals critical plasticity in immune response. Mol. Syst. Biol. *6*, 437. https://doi.org/10.1038/msb.2010.90.
5. Park, J.H., Yu, Q., Erman, B., Appelbaum, J.S., Montoya-Durango, D., Grimes, H.L., and Singer, A. (2004). Suppression of IL7Ralpha transcription by IL-7 and other prosurvival cytokines: a novel mechanism for maximizing IL-7-dependent T cell survival. Immunity *21*, 289–302. https://doi.org/10.1016/j.immuni.2004.07.016.
6. Leonard, W.J., and Lin, J.-X. (2023). Strategies to therapeutically modulate cytokine action. Nat. Rev. Drug Discov. *22*, 827–854. https://doi.org/10.1038/s41573-023-00746-x.
7. Hernandez, R., Põder, J., LaPorte, K.M., and Malek, T.R. (2022). Engineering IL-2 for immunotherapy of autoimmunity and cancer. Nat. Rev. Immunol. *22*, 614–628. https://doi.org/10.1038/s41577-022-00680-w.
8. Chen, D., Tang, T.-X., Deng, H., Yang, X.-P., and Tang, Z.-H. (2021). Interleukin-7 Biology and Its Effects on Immune Cells: Mediator of Generation, Differentiation, Survival, and Homeostasis. Front. Immunol. *12*, 747324. https://doi.org/10.3389/fimmu.2021.747324.
9. Klatzmann, D., and Abbas, A.K. (2015). The promise of low-dose interleukin-2 therapy for autoimmune and inflammatory diseases. Nat. Rev. Immunol. *15*, 283–294. https://doi.org/10.1038/nri3823.
10. Ditoro, D., Winstead, C.J., Pham, D., Witte, S., Andargachew, R., Singer, J.R., Wilson, C.G., Zindl, C.L., Luther, R.J., Silberger, D.J., et al. (2018). Differential IL-2 expression defines developmental fates of follicular versus nonfollicular helper T cells. Science *361*, eaao2933. https://doi.org/10.1126/science.aao2933.
11. Crank, J. (1979). The Mathematics of Diffusion (Oxford university press).
12. Busse, D., de la Rosa, M., Hobiger, K., Thurley, K., Flossdorf, M., Scheffold, A., and Höfer, T. (2010). Competing feedback loops shape IL-2 signaling between helper and regulatory T lymphocytes in cellular microenvironments. Proc. Natl. Acad. Sci. USA *107*, 3058–3063. https://doi.org/10.1073/pnas.0812851107.
13. Thurley, K., Gerecht, D., Friedmann, E., and Höfer, T. (2015). Three-Dimensional Gradients of Cytokine Signaling between T Cells. PLoS Comput. Biol. *11*, e1004206. https://doi.org/10.1371/journal.pcbi.1004206.
14. Fuhrmann, F., Lischke, T., Gross, F., Scheel, T., Bauer, L., Kalim, K.W., Radbruch, A., Herzel, H., Hutloff, A., and Baumgrass, R. (2016). Adequate immune response ensured by binary IL-2 and graded CD25 expression in a murine transfer model. Elife *5*, e20616. https://doi.org/10.7554/eLife.20616.
15. Wong, H.S., Park, K., Gola, A., Baptista, A.P., Miller, C.H., Deep, D., Lou, M., Boyd, L.F., Rudensky, A.Y., Savage, P.A., et al. (2021). A local regulatory T cell feedback circuit maintains immune homeostasis by pruning self-activated T cells. Cell *184*, 3981–3997.e22. https://doi.org/10.1016/j.cell.2021.05.028.
16. Oyler-Yaniv, A., Oyler-Yaniv, J., Whitlock, B.M., Liu, Z., Germain, R.N., Huse, M., Altan-Bonnet, G., and Krichevsky, O. (2017). A Tunable Diffusion-Consumption Mechanism of Cytokine Propagation Enables Plasticity in Cell-to-Cell Communication in the Immune System. Immunity *46*, 609–620. https://doi.org/10.1016/J.IMMUNI.2017.03.011.
17. Altan-Bonnet, G., and Mukherjee, R. (2019). Cytokine-mediated communication: a quantitative appraisal of immune complexity. Nat. Rev. Immunol. *19*, 205–217. https://doi.org/10.1038/s41577-019-0131-x.
18. Liu, Z., Gerner, M.Y., Van Panhuys, N., Levine, A.G., Rudensky, A.Y., and Germain, R.N. (2015). Immune homeostasis enforced by co-localized effector and regulatory T cells. Nature *528*, 225–230. https://doi.org/10.1038/nature16169.
19. Höfer, T., Krichevsky, O., and Altan-Bonnet, G. (2012). Competition for IL-2 between regulatory and effector T cells to chisel immune responses. Front. Immunol. *3*, 1–9. https://doi.org/10.3389/fimmu.2012.00268.
20. Maire, T., and Youk, H. (2015). Molecular-Level Tuning of Cellular Autonomy Controls the Collective Behaviors of Cell Populations. Cell Syst. *1*, 349–360. https://doi.org/10.1016/j.cels.2015.10.012.
21. Berg, H.C., and Purcell, E.M. (1977). Physics of chemoreception. Biophys. J. *20*, 193–219. https://doi.org/10.1016/S0006-3495(77)85544-6.
22. Prabhakar, U., Eirikis, E., Reddy, M., Silvestro, E., Spitz, S., Pendley, C., Davis, H.M., and Miller, B.E. (2004). Validation and comparative analysis of a multiplexed assay for the simultaneous quantitative measurement of Th1/Th2 cytokines in human serum and human peripheral blood mononuclear cell culture supernatants. J. Immunol. Methods *291*, 27–38. https://doi.org/10.1016/j.jim.2004.04.018.
23. Wang, H.M., and Smith, K.A. (1987). The interleukin 2 receptor: Functional consequences of its bimolecular structure. J. Exp. Med. *166*, 1055–1069. https://doi.org/10.1084/jem.166.4.1055.
24. Cotari, J.W., Voisinne, G., Dar, O.E., Karabacak, V., and Altan-Bonnet, G. (2013). Cell-to-cell variability analysis dissects the plasticity of signaling of common γ chain cytokines in T cells. Sci. Signal. *6*, ra17. https://doi.org/10.1126/scisignal.2003240.
25. Han, Q., Bagheri, N., Bradshaw, E.M., Hafler, D.A., Lauffenburger, D.A., and Love, J.C. (2012). Polyfunctional responses by human T cells result from sequential release of cytokines. Proc. Natl. Acad. Sci. USA *109*, 1607–1612. https://doi.org/10.1073/pnas.1117194109.
26. Podtschaske, M., Benary, U., Zwinger, S., Höfer, T., Radbruch, A., and Baumgrass, R.

(2007). Digital NFATc2 Activation per Cell Transforms Graded T Cell Receptor Activation into an All-or-None IL-2 Expression. PLoS One *2*, e935. https://doi.org/10.1371/journal.pone.0000935.
27. Fajgenbaum, D.C., and June, C.H. (2020). Cytokine Storm. N. Engl. J. Med. *383*, 2255–2273. https://doi.org/10.1056/NEJMra2026131.
28. Tisoncik, J.R., Korth, M.J., Simmons, C.P., Farrar, J., Martin, T.R., and Katze, M.G. (2012). Into the Eye of the Cytokine Storm. Microbiol. Mol. Biol. Rev. *76*, 16–32. https://doi.org/10.1128/MMBR.05015-11.
29. Long, M., and Adler, A.J. (2006). Cutting Edge: Paracrine, but Not Autocrine, IL-2 Signaling Is Sustained during Early Antiviral CD4 T Cell Response. J. Immunol. *177*, 4257–4261. https://doi.org/10.4049/jimmunol.177.7.4257.
30. Tkach, K.E., Barik, D., Voisinne, G., Malandro, N., Hathorn, M.M., Cotari, J.W., Vogel, R., Merghoub, T., Wolchok, J., Krichevsky, O., and Altan-Bonnet, G. (2014). T cells translate individual, quantal activation into collective, analog cytokine responses via time-integrated feedbacks. Elife *3*, e01944. https://doi.org/10.7554/eLife.01944.
31. Kim, H.P., Kelly, J., and Leonard, W.J. (2001). The Basis for IL-2-Induced IL-2 Receptor α Chain Gene Regulation: Importance of Two Widely Separated IL-2 Response Elements. Immunity *15*, 159–172. https://doi.org/10.1016/S1074-7613(01)00167-4.
32. Cheng, G., Yu, A., and Malek, T.R. (2011). T-cell tolerance and the multi-functional role of IL-2R signaling in T-regulatory cells: IL-2R signaling and Treg cell function. Immunol. Rev. *241*, 63–76. https://doi.org/10.1111/j.1600-065X.2011.01004.x.
33. Ghazawi, F.M., Faller, E.M., Sugden, S.M., Kakal, J.A., and MacPherson, P.A. (2013). IL-7 downregulates IL-7Rα expression in human CD8 T cells by two independent mechanisms. Immunol. Cell Biol. *91*, 149–158. https://doi.org/10.1038/icb.2012.69.
34. Dustin, M.L. (2014). The Immunological Synapse. Cancer Immunol. Res. *2*, 1023–1033. https://doi.org/10.1158/2326-6066.CIR-14-0161.
35. Grakoui, A., Bromley, S.K., Sumen, C., Davis, M.M., Shaw, A.S., Allen, P.M., and Dustin, M.L. (1999). The immunological synapse: A molecular machine controlling T cell activation. Science *285*, 221–227. https://doi.org/10.1126/science.285.5425.221.
36. Thurley, K., Wu, L.F., and Altschuler, S.J. (2018). Modeling Cell-to-Cell Communication Networks Using Response-Time Distributions. Cell Syst. *6*, 355–367.e5. https://doi.org/10.1016/J.CELS.2018.01.016.
37. Burt, P., and Thurley, K. (2023). Distribution modeling quantifies collective TH cell decision circuits in chronic inflammation. Sci. Adv. *9*, eadg7668.
38. Onder, L., Narang, P., Scandella, E., Chai, Q., Iolyeva, M., Hoorweg, K., Halin, C., Richie, E., Kaye, P., Westermann, J., et al. (2012). IL-7–producing stromal cells are critical for lymph node remodeling. Blood *120*, 4675–4683. https://doi.org/10.1182/blood-2012-03-416859.
39. Park, J.H., Waickman, A.T., Reynolds, J., Castro, M., and Molina-París, C. (2019). IL7 receptor signaling in T cells: A mathematical modeling perspective. Wiley Interdiscip. Rev. Syst. Biol. Med. *11*, e1447. https://doi.org/10.1002/wsbm.1447.
40. Eisenbarth, S.C. (2019). Dendritic cell subsets in T cell programming: location dictates function. Nat. Rev. Immunol. *19*, 89–103. https://doi.org/10.1038/s41577-018-0088-1.
41. Grant, S.M., Lou, M., Yao, L., Germain, R.N., and Radtke, A.J. (2020). The lymph node at a glance – how spatial organization optimizes the immune response. J. Cell Sci. *133*, jcs241828. https://doi.org/10.1242/jcs.241828.
42. Sakaguchi, S., Mikami, N., Wing, J.B., Tanaka, A., Ichiyama, K., and Ohkura, N. (2020). Regulatory T Cells and Human Disease. Annu. Rev. Immunol. *38*, 541–566. https://doi.org/10.1146/annurev-immunol-042718-041717.
43. Bacher, P., Heinrich, F., Stervbo, U., Nienen, M., Vahldieck, M., Iwert, C., Vogt, K., Kollet, J., Babel, N., Sawitzki, B., et al. (2016). Regulatory T Cell Specificity Directs Tolerance versus Allergy against Aeroantigens in Humans. Cell *167*, 1067–1078.e16. https://doi.org/10.1016/j.cell.2016.09.050.
44. Daneshpour, H., and Youk, H. (2019). Modeling cell–cell communication for immune systems across space and time. Curr. Opin. Syst. Biol. *18*, 44–52. https://doi.org/10.1016/J.COISB.2019.10.008.
45. Dang, Y., Grundel, D.A.J., and Youk, H. (2020). Cellular Dialogues: Cell-Cell Communication through Diffusible Molecules Yields Dynamic Spatial Patterns. Cell Syst. *10*, 82–98.e7. https://doi.org/10.1016/j.cels.2019.12.001.
46. Berg, O.G. (1978). On diffusion-controlled dissociation. Chem. Phys. *31*, 47–57. https://doi.org/10.1016/0301-0104(78)87025-6.
47. Fange, D., Berg, O.G., Sjöberg, P., and Elf, J. (2010). Stochastic reaction-diffusion kinetics in the microscopic limit. Proc. Natl. Acad. Sci. USA *107*, 19820–19825. https://doi.org/10.1073/pnas.1006565107.
48. Yanagihara, Y., Ikizawa, K., Kajiwara, K., Koshio, T., Basaki, Y., and Akiyama, K. (1995). Functional significance of IL-4 receptor on B cells in IL-4-induced human IgE production. J. Allergy Clin. Immunol. *96*, 1145–1151. https://doi.org/10.1016/S0091-6749(95)70199-0.
49. Monteleone, G., Monteleone, I., Fina, D., Vavassori, P., Del Vecchio Blanco, G., Caruso, R., Tersigni, R., Alessandroni, L., Biancone, L., Naccari, G.C., et al. (2005). Interleukin-21 enhances T-helper cell type I signaling and interferon-γ production in Crohn's disease. Gastroenterology *128*, 687–694. https://doi.org/10.1053/j.gastro.2004.12.042.
50. Duan, D., and Derynck, R. (2019). Transforming growth factor–β (TGF-β)–induced up-regulation of TGF-β receptors at the cell surface amplifies the TGF-β response. J. Biol. Chem. *294*, 8490–8504. https://doi.org/10.1074/jbc.RA118.005763.
51. Alon, U. (2007). Network motifs: theory and experimental approaches. Nat. Rev. Genet. *8*, 450–461. https://doi.org/10.1038/nrg2102.
52. Rosenfeld, N., Elowitz, M.B., and Alon, U. (2002). Negative Autoregulation Speeds the Response Times of Transcription Networks. J. Mol. Biol. *323*, 785–793. https://doi.org/10.1016/S0022-2836(02)00994-4.
53. Meyer-Hermann, M., Mohr, E., Pelletier, N., Zhang, Y., Victora, G.D., and Toellner, K.-M. (2012). A Theory of Germinal Center B Cell Selection, Division, and Exit. Cell Rep. *2*, 162–174. https://doi.org/10.1016/j.celrep.2012.05.010.
54. Beltman, J.B., Allen, C.D.C., Cyster, J.G., and De Boer, R.J. (2011). B cells within germinal centers migrate preferentially from dark to light zone. Proc. Natl. Acad. Sci. USA *108*, 8755–8760. https://doi.org/10.1073/pnas.1101554108.
55. Wortel, I.M.N., and Textor, J. (2023). Interpreting T-cell search "strategies" in the light of evolution under constraints. PLoS Comput. Biol. *19*, e1010918. https://doi.org/10.1371/journal.pcbi.1010918.
56. Van Der Hoorn, I.A.E., Martynova, E., Subtil, B., Meek, J., Verrijp, K., Textor, J., Flórez-Grau, G., Piet, B., Van Den Heuvel, M.M., De Vries, I.J.M., and Gorris, M.A.J. (2024). Detection of dendritic cell subsets in the tumor microenvironment by multiplex immunohistochemistry. Eur. J. Immunol. *54*, 2350616. https://doi.org/10.1002/eji.202350616.
57. Pascual-Reguant, A., Köhler, R., Mothes, R., Bauherr, S., Hernández, D.C., Uecker, R., Holzwarth, K., Kotsch, K., Seidl, M., Philipsen, L., et al. (2021). Multiplexed histology analyses for the phenotypic and spatial characterization of human innate lymphoid cells. Nat. Commun. *12*, 1737. https://doi.org/10.1038/s41467-021-21994-8.
58. Lin, J.-R., Wang, S., Coy, S., Chen, Y.-A., Yapp, C., Tyler, M., Nariya, M.K., Heiser, C.N., Lau, K.S., Santagata, S., and Sorger, P.K. (2023). Multiplexed 3D atlas of state transitions and immune interaction in colorectal cancer. Cell *186*, 363–381.e19. https://doi.org/10.1016/j.cell.2022.12.028.
59. Cendrowski, J., Mamińska, A., and Miaczynska, M. (2016). Endocytic regulation of cytokine receptor signaling. Cytokine Growth Factor Rev. *32*, 63–73. https://doi.org/10.1016/j.cytogfr.2016.07.002.
60. Hémar, A., Subtil, A., Lieb, M., Morelon, E., Hellio, R., and Dautry-Varsat, A. (1995). Endocytosis of interleukin 2 receptors in human T lymphocytes: distinct intracellular localization and fate of the receptor alpha, beta, and gamma chains. J. Cell Biol. *129*, 55–64. https://doi.org/10.1083/jcb.129.1.55.
61. Conway, E., Hoff, D., and Smoller, J. (1978). Large Time Behavior of Solutions of Systems of Nonlinear Reaction-Diffusion Equations. SIAM J. Appl. Math. *35*, 1–16. https://doi.org/10.1137/0135001.
62. Alnaes, M.S., Blechta, J., Hake, J., Johansson, A., Kehlet, B., Logg, A., Richardson, C., Ring, J., Rognes, M.E., and Wells, G.N. (2015). The FEniCS Project Version 1.5. Arch. Numer. Softw. *3*, 9–23.
63. Geuzaine, C., and Remacle, J.-F. (2009). Gmsh: A 3-D finite element mesh generator with built-in pre- and post-processing facilities. Int. J. Numer. Methods Eng. *79*, 1309–1331. https://doi.org/10.1002/nme.2579.
64. Bridson, R. (2007). Fast Poisson Disk Sampling in Arbitrary Dimensions. In ACM SIGGRAPH 2007 Sketches SIGGRAPH '07 (Association for Computing Machinery), pp. 22–es. https://doi.org/10.1145/1278780.1278807.
65. Ashman, K.A., Bird, C.M., and Zepf, S.E. (1994). Detecting bimodality in astronomical datasets. Astron. J. *108*, 2348. https://doi.org/10.1086/117248.

STAR★METHODS

KEY RESOURCES TABLE

REAGENT or RESOURCE	SOURCE	IDENTIFIER
Software and algorithms		
FEniCS	FEniCS Project	http://www.fenicsproject.org/
Gmsh	Gmsh Project	https://gmsh.info/
SciPy	SciPy Project	https://scipy.org/
Simulation and data analysis code	This paper	https://doi.org/10.5281/zenodo.11127473

RESOURCE AVAILABILITY

Lead contact

Further information and requests for resources should be directed to and will be fulfilled by the lead contact, Kevin Thurley (kevin.thurley@uni-bonn.de).

Materials availability

This study did not generate any new materials.

Data and code availability

- All the information about the data reported here is included in this paper.
- All computer code generated in the study can be found under the following url: https://doi.org/10.5281/zenodo.11127473.
- Any additional information required to reanalyze the data reported in this paper is available from the lead contact upon request.

METHOD DETAILS

Mathematical models

Core-model of spatially resolved cytokine dynamics

Let Ω be the extracellular space, Θ the outer boundary of that space and $\Gamma_i, i = 1,\ldots,N_{\text{cells}}$, denote the cell-surfaces. In all simulations, for each cytokine considered, we assumed the cytokine concentration $c(x)$, $x \in \Omega$ to be in quasi-steady-state, and we imposed no-flux conditions at the outer boundary, that is $\frac{\partial c}{\partial \vec{n}} = 0$ on Θ where $\vec{n}$ is the normal vector on the cells surface pointing toward the extracellular space. Further, assuming homogeneous cytokine secretion and uptake on each cell-surface with area A_i, the interaction between a cell and the extracellular cytokine concentration is realized through generalized Robin boundary conditions (cf. Ref.[12,13]):

$$0 = D\Delta c - \eta c \text{ in } \Omega \qquad \text{(Equation 1)}$$

$$\frac{\partial c}{\partial \vec{n_i}} = \frac{q_i}{A_i D} - \frac{\Psi_i(c)}{A_i D} \text{ on } \Gamma_i$$

Here, D is the diffusion coefficient, η is a homogeneous decay rate and Δ is the three-dimensional Laplace operator. For the sake of simplicity, we assume a uniform cell-size $A_i := A_{\text{cell}}$ throughout. Furthermore, we take the secretion rate q_i and the surface concentration as average values across the cell-surface for each cell, that is $c_i := \frac{1}{A_{\text{cell}}}\int_{\Gamma_i} c\,ds$. Hence, the uptake rate takes the form

$$\Psi_i(c_i) = k_{\text{endo}} R_i\, f(c_i) \qquad \text{(Equation 2)}$$

where R_i denotes the number of receptors expressed on the cell-surface. In the case of linear cytokine uptake, the uptake function takes the form $f(c_i) = \frac{k_{\text{on}}}{k_{\text{off}}} c_i$, where k_{on} is the cytokine-receptor association rate.[12,13] A more realistic description of cytokine uptake takes into account that the uptake capacity of a cell is limited not only by the amount of receptors expressed on the surface, but also by the intracellular machinery for cytokine degradation and 'recycling' of cytokine receptors.[12,59,60] That results in an uptake function of the form $f(c_i) = \frac{c_i}{K_D + c_i}$, where K_D is the half-saturation constant for cytokine uptake. We found that this form of the uptake function can be justified by a mechanistic, Michaelis-Menten type description of cytokine-binding to its receptor (Method details, "Description of saturated uptake dynamics"). Further, assuming $k_{\text{endo}} = k_{\text{off}}$, we retrieve the canonical form of the linear uptake function $\Psi_i(c_i) = k_{\text{on}} R_i\, c_i$. In the case of non-secretory responder cells, we set $q_i = 0$ in Equation 1 and $R_i = R_{resp}$ in Equation 2, whereas we take $q_i = q_{sec}$ and $R_i = R_{sec}$ for cytokine-secreting cells. The latter ones express

lower numbers of cytokine receptors and thus exhibit a reduced uptake rate $\Psi_i(c_i)$ (cf. Table 1). Moreover, we account for receptor heterogeneity on responding cells (Figure 2) by sampling R_i from a log-normal distribution with mean R_{resp}.

As a primary output of our model simulations, we assess cellular activation in terms of the fraction of phosphorylated STAT5, which we take as

$$\mathrm{pSTAT5}(c,R) = \frac{c^H}{\mathrm{EC50}(R)^H + c^H}, H = 3. \quad \text{(Equation 3)}$$

A cell is considered activated if its pSTAT5 level reaches values $\mathrm{pSTAT5}(c_i,R_i) \geq 0.5$. In line with experimental data,[24] we account for a dependency of the EC50 value on the level of receptor expression through $\mathrm{EC50}(R) = \frac{E_{\max} k^N + E_{\min} R^N}{k^N + R^N}$, where $E_{\max}$, $E_{\min}$, k and N are parameters determined through fitting of experimental data extracted from Cotari et al., Figure 3A.[24] Model parameters (Table 1) could in many cases be assigned to or derived from published experiments.

Receptor feedback kinetics

In order to analyze the delayed receptor feedback introduced in Figure 3, we considered a time-dependent change in receptors, leading to a time-dependent cytokine distribution. That is, our quasi-stationary diffusion problem, Equation 1, is generalized to a series of such problems, via $\Psi_i(c_i) = \Psi_i(c_i(t), R_i(t))$ in Equation 2, given by a system of ODEs for receptor expression in each cell:

$$\frac{dR_i}{dt} = g_i(c_i, R_i) \quad \text{(Equation 4)}$$

Specifically, we chose a receptor feedback function

$$g_i(c_i,R_i) = \frac{k_{\mathrm{base}} K_m^N + \gamma_i k_{\mathrm{base}}\, \mathrm{pSTAT5}(c_i,R_i)^N}{K_m^N + \mathrm{pSTAT5}(c_i,R_i)^N} - \nu R_i \quad \text{(Equation 5)}$$

that depends on the cellular pSTAT5 level, the minimal receptor production rate k_{base}, the half saturation value for activation K_m and the receptor decay rate ν. The feedback fold change γ_i depends on the cell type, here we take $\gamma_i = 1$ for cytokine-secreting cells, $\gamma_i \in (1, 100]$ for positive and $\gamma_i \in [0.01, 1)$ for negative feedback on responding cells. For visualization, to allow for a unified x-axis, the fold change for negative feedback was inverted. To account for delayed regulation of receptor expression on the responding cell i caused by intracellular processes such as signal transduction and gene expression, we supplemented Equation 4 by equations for auxiliary states ('linear chain trick', cf. Figure S4A), as previously described:[37]

$$0 = D\Delta c - \eta c \text{ in } \Omega \quad \text{(Equation 6)}$$

$$\frac{\partial c}{\partial \vec{n_i}} = \frac{q_i}{A_i D} - \frac{\Psi_i(c_i,R_i)}{A_i D} \text{ on } \Gamma_i$$

$$\frac{dR_i^{(*)}}{dt} = g_i\left(c_i, R_i^{(*)}\right)$$

$$\frac{dx_{i,l}}{dt} = \lambda(x_{i,l-1} - x_{i,l}), l = 2, \ldots M, x_{i,1} = R_i^{(*)}, R_i := x_{i,M}$$

Well-mixed model

In the well-mixed case, i.e. assuming infinitely fast diffusion, the homogeneous extracellular cytokine distribution is described by an ODE. Namely, by neglecting the cell volumes, the core PDE model (Equation 1) converges for $D \to \infty$ to an ODE in terms of the system-wide quantities $q_{tot} := q_{sec} N_{sec}$, where N_{sec} denotes the number of secreting cells, and $\Psi_{tot}(c) := k_{\mathrm{endo}} R_{tot} f(c)$ with $R_{tot} := N_{sec} R_{sec} + N_{resp} R_{resp}$, considered at steady-state (Section "Mathematical derivations: Deriving the well-mixed model"):[61]

$$0 = q_{tot} - \Psi_{tot}(\bar{c}) - \eta \bar{c}. \quad \text{(Equation 7)}$$

As in the core PDE model, we have $f(c) = \frac{k_{on}}{k_{off}} c$ for linear uptake and $f(c) = \frac{c}{K_D + c}$ for saturated uptake. Parameters were chosen identically to the core model and are listed in Table 1.

Furthermore, the steady-state solution $\bar{c}$ of the well-mixed ODE is the average of the cytokine distribution c described by the core PDE,[61] i.e. $\bar{c} = \frac{1}{|\Omega|}\int_\Omega c(x)dx$. That allows for a direct comparison to the core model in terms of analytical expression of values for the average cytokine concentration (see Method details).

Analogous to the core PDE model, we introduced delayed receptor feedback in the well-mixed model by a time-dependent uptake function $\Psi_{tot}(c) = \Psi_{tot}(c(t), R_{tot}(t))$ and receptor expression dynamics $\frac{dR_{tot}}{dt} = g(c, R_{tot})$.

Software and simulations

Numerics

All spatial simulations are carried out using the finite-element solver FEniCS[62] with P1 elements, a generalized minimal residual methods (GMRES) solver and algebraic multi grid (AMG) preconditioner. The solution accuracy is controlled by the Krylov solver tolerance for linear and the Newton solver tolerance for the non-linear boundary conditions. A description of the weak formulation of the models used therein is provided below (Section "Mathematical derivations: Deriving the weak form"). Standard parameter values are listed in Table 1. The extracellular space was discretized as a uniform tetrahedral mesh using Gmsh,[63] the mesh fidelity was chosen to yield a mesh with approximately 100,000 degrees of freedom in a cube of 240 μm edge length. To minimize boundary effects the outermost layer of cells is disregarded in our analysis. The ODE model arising in the well-mixed scenario was solved using a SciPy ODE solver.

Random cell positioning and cell-type clustering

To achieve an efficient 3-dimensional random cell positioning (cf. Figure 5), we utilize Bridson sampling, a Poisson disk sampling approach.[64] The algorithm achieves a dense packing of cell centroids in two or three dimensions while respecting a minimum distance r to account for the physical dimension of the cells, by iteratively adding new points draw from uniform distributions that span the $[r, 2r]$ spherical shell around the existing points. The average cell-cell distance and the amount of sampling steps are chosen to yield the same average cell density as in the grid approach employed in all other simulations (Figures 1, 2, 3, and 4). Further, in order to achieve the high density of secreting cells around APCs in Figure 5, we developed an algorithm that assigns cell type identities to the existing cell locations of the pre-generated mesh with different fraction and clustering strength for each cell type. In a first step, a cell density is computed using kernel density estimation (KDE) from the APC locations. For each cell type, cell identities are assigned independently with a probability proportional to the density value at each location. In a second step, conflicts are iteratively resolved by a stochastic approach that is a biased towards the cell type with higher clustering strength.

Mathematical derivations

Deriving the weak form

In order to numerically solve the partial differential equation (PDE) posed in Equation 1, one first has to derive the weak form. Let $\Omega \subset \mathbb{R}^3$ be the extracellular space, $\Theta \subset \mathbb{R}^2$ be the outer boundary of that space and $\Gamma_i \subset \mathbb{R}^2,\ i = 1, \ldots, N_{\text{cells}}$ the closed boundaries for every cell.

$$0 = D\Delta c - \eta c = D\nabla^2 c - \eta c \qquad \text{(Equation 8)}$$

$$\frac{\partial c}{\partial \vec{n}} = 0 \text{ on } \Theta \qquad \text{(Equation 9)}$$

$$\frac{\partial c}{\partial \vec{n}_i} = \frac{q_i}{A_i D} - \frac{\Psi_i(c_i)}{A_i D} \text{ on } \Gamma_i \qquad \text{(Equation 10)}$$

To derive the weak formulation necessary to solve this problem, we multiply Equation 8 by a test function v and integrate over the extracellular space Ω, yielding

$$D\int_\Omega (\nabla^2 c) v \, dx = \int_\Omega \eta c \cdot v \, dx \qquad \text{(Equation 11)}$$

with dx as the differential element for the integration over Ω. Utilizing integration by parts and the divergence theorem, we can write the left side of this equation as

$$D\int_\Omega (\nabla^2 c) v \, dx = -D\int_\Omega \nabla c \cdot \nabla v \, dx + D\int_{\partial\Omega} \frac{\partial c}{\partial \vec{n}} v \, ds \qquad \text{(Equation 12)}$$

with ds as the differential element for the integration over all boundaries of Ω. Using Equations 9 and 10 the integration over the boundary $\partial\Omega$ can be written as

$$\int_{\partial\Omega} \frac{\partial c}{\partial \vec{n}} v \, ds = \int_\Theta \underbrace{\frac{\partial c}{\partial \vec{n}}}_{=0} v \, ds + \sum_i \int_{\Gamma_i} \frac{\partial c}{\partial \vec{n}_i} v \, ds = \sum_i \int_{\Gamma_i} \frac{1}{A_i D} \left(q_i - \Psi_i(c_i)\right) v \, ds$$

$$= \sum_i \frac{1}{D} \left(q_i - \Psi_i(c_i)\right) v. \qquad \text{(Equation 13)}$$

With this we get the weak form

$$D\int_{\Omega}\nabla c\cdot\nabla v\,dx = -\int_{\Omega}\eta c\cdot v\,dx+\sum_{i}(q_i - \Psi_i(c_i))v \quad \text{(Equation 14)}$$

which we use in FEniCS[62] to solve the RD-system.

Deriving the well-mixed model

To evaluate the spatial effects in the PDE based core model we compare our results with the ordinary differential equation (ODE) based well-mixed model (cf. Figure 1). The ODE approach does not include spatial information but rather assumes that the extracellular volume is well-mixed. Mathematically this can be achieved by neglecting the cell volumes, leading to cytokine secretion and uptake to be considered system-wide with respective rates

$$q_{\text{tot}} = D\sum_{\text{sec.}}\sum_{\text{cells }i}\int_{\Gamma_i}\frac{q_i}{A_iD}ds = q_{\text{sec}}N_{\text{sec}} \quad \text{(Equation 15)}$$

$$\Psi_{\text{tot}}(c) = D\sum_{\text{cells }i}\int_{\Gamma_i}\frac{\Psi_i(c)}{A_iD}ds = \sum_{\text{cells }i}\Psi_i(c) = \begin{cases} k_{\text{on}}R_{\text{tot}}c & \text{linear} \\ k_{\text{endo}}R_{\text{tot}}\frac{c}{K_D+c} & \text{saturated.}\end{cases} \quad \text{(Equation 16)}$$

Thus, the core PDE in Equation 8 with neglected cell volumes can be written as

$$0 = D\Delta c - \eta c + q_{\text{tot}} - \Psi_{\text{tot}}(c) \text{ in } \Omega \quad \text{(Equation 17)}$$

$$\frac{\partial c}{\partial\overrightarrow{n}} = 0 \text{ on } \Theta \quad \text{(Equation 18)}$$

Using Gronwall estimations, it was shown that for $D\to\infty$, the solution c of Equation 17 converges exponentially to its space average $\overline{c} = \frac{1}{|\Omega|}\int_{\Omega}c(x)\,dx$.[61] This yields the well-mixed ODE at steady-state, solving Equation 8 as

$$\overline{c} = \frac{q_{\text{sec}}N_{\text{sec}}}{k_{\text{on}}R_{\text{tot}}+\eta} \quad \text{(Equation 19)}$$

in case of the linear uptake and

$$\overline{c} = \frac{q_{\text{tot}} - k_{\text{endo}}R_{\text{tot}} - K_D\eta+\sqrt{K_D^2\eta^2+2K_D\eta(q_{\text{tot}}+k_{\text{endo}}R_{\text{tot}})+(q_{\text{tot}} - k_{\text{endo}}R_{\text{tot}})^2}}{2\eta} \quad \text{(Equation 20)}$$

In the case of saturated uptake.

Description of saturated uptake dynamics

To account for saturating effects in our uptake dynamics, we employ classical Michaelis-Menten kinetics in order to find the uptake function Ψ described in the methods in the main text. The binding of cytokine c to a receptor R, formation of a cytokine/receptor complex followed by internalization can be written as

$$c+R\underset{k_{\text{off}}}{\overset{k_{\text{on}}}{\rightleftarrows}}C\overset{k_{\text{endo}}}{\to}P \quad \text{(Equation 21)}$$

with C as cytokine/receptor complexes and P as the internalized cytokine/receptor complexes with their corresponding rates k_{on} for binding, k_{off} for unbinding, and k_{endo} for endocytosis.

From this, we can define the differential equations as

$$\begin{aligned}\frac{dR}{dt} &= k_{\text{off}}C - k_{\text{on}}Rc + a \\ \frac{dC}{dt} &= k_{\text{on}}Rc - k_{\text{off}}C - k_{\text{endo}}C\end{aligned} \quad \text{(Equation 22)}$$

with a as a base receptor production. Under the assumptions that $c \gg R$ and $P_0 = 0$, the uptake flux Ψ can be considered as the velocity at which C is converted into P, resulting in

$$\Psi = k_{\text{endo}}C \quad \text{(Equation 23)}$$

Under the rapid equilibrium assumption we assume that the rate at which equilibrium between cytokine/receptor binding and unbinding is reached is fast compared to the rate at which the complex C forms the product P, we get

$$k_{on} R c = k_{off} C \quad \text{(Equation 24)}$$

and employing mass conservation $R = R_0 - C$, where R is the number of unbound receptors on the cell and R_0 is the overall amount of receptors, we get

$$C = \frac{k_{on} R_0 c}{k_{off} + k_{on} c} = \frac{R_0 c}{K_D + c}. \quad \text{(Equation 25)}$$

With this we can write Equation 23 as

$$\Psi(c, R_0) = k_{endo} C = k_{endo} R_0 \frac{c}{K_D + c}. \quad \text{(Equation 26)}$$

Here $\Psi(c, R)$ is linear in R and saturates via a Hill-function in c.

Description of linear uptake dynamics

To systematically analyze the previously described saturated uptake dynamic, we also derived an uptake function linear in c, which we use in Figure S3 to delineate saturation effects. Assuming $c \ll K_D$ with $K_D = \frac{k_{off}}{k_{on}}$, we can simplify Equation 26 as

$$\Psi(c, R_0) = k_{endo} R_0 \frac{c}{K_D + c} = k_{endo} R_0 \frac{c}{\frac{k_{off}}{k_{on}} + c} \approx k_{endo} R_0 \frac{c}{\frac{k_{off}}{k_{on}}} = \frac{k_{endo}}{k_{off}} k_{on} R_0 c \quad \text{(Equation 27)}$$

If we further assume $k_{endo} = k_{off}$, it simplifies to

$$\Psi(c, R_0) = k_{on} R_0 c \quad \text{(Equation 28)}$$

resulting in a function that scales linearly with c.

As expected, the saturated uptake function is well approximated by Equation 28 for low cytokine concentrations c (Figure S3D), in particular if $c \ll K_D$ holds. For high cytokine secretion rates, the saturated uptake function results in larger cytokine concentration levels, and since c depends on K_D, it is not possible to fix the system in a linear regime by increasing K_D alone (cf. Figure 2B). To highlight this dependence, consider the saturated well-mixed case (cf. Equation 7) with $\eta = 0$:

$$0 = q_{tot} - k_{endo} R_{tot} \frac{c}{K_D + c} \quad \text{(Equation 29)}$$

$$\Rightarrow c = \frac{q_{tot} \cdot K_D}{k_{endo} R_{tot} - q_{tot}} \quad \text{(Equation 30)}$$

Here c is directly proportional to K_D, so any increase in K_D will yield the same increase in c. To fulfill the condition $c \ll K_D$, we can decrease q, and hence q_{tot}, yielding a linear decrease in c since $k_{endo} R_{tot}$ remains constant. Thus, in the well-mixed model, our saturated uptake dynamics transition into the linear regime for low cytokine secretion rates only, while in the spatial RD-system, the cytokine concentration c decays with increased distance to a secreting cell (cf. Figure 1B), resulting in the gradual transition from saturated to linear uptake observed in Figure S3D.

Analytical approximation of the cytokine concentration field

The analytical approximation, taken from Thurley et al.[13] and used to validate our results in Figure S1 and S3, calculates the cytokine concentration for an environment with a high density of responding cells around a single secreting cell. It also assumes radial symmetry and is defined as

$$c(r) = \frac{q\rho}{k_{on} r} \frac{4\pi D r(L+\rho) + k_{on}(L - r + \rho) N R}{k_{on} L R_{sec} N R + 4\pi D \rho (L+\rho)(R_{sec} + N R)} \quad \text{(Equation 31)}$$

with ρ as the cell radius, L as the synaptic distance, N as the number of IL-2 consuming responder cells and R_{sec} as the receptors on secreting cells. Since the standard setup in our core model uses multiple cytokine secreting cells which are not necessarily isolated, this solution can only be used to approximate the cytokine concentration in this scenario.

QUANTIFICATION AND STATISTICAL ANALYSIS

Statistics

The surface concentration average and the spatial standard deviation (s.d.) were computed using the surface concentration values of all cells in one configuration. The gradient refers to the sum of the cytokine gradients in the extracellular space and was computed through the average norm of the cytokine field gradient. The Spearman rank-order correlation coefficient (r_s) was computed using SciPy. To quantify the bimodality of a distribution we calculated the relative separation using Ashman's D.[65] Quantitative analysis of stochastic simulations was performed by taking the average and standard error of the mean (SEM) across multiple runs, as described in Figure legends.

Quantifying spatial patterns: Niche score, niche effect and signaling range

To calculate the niche score and niche effect in Figure 4, it is necessary to determine which pSTAT5^{+} cells are being activated by which secreting cell. This is achieved by running the DBSCAN algorithm with all pSTAT5^{+} and secreting cells spatial coordinates as input and the average cell-cell distance, typically 20 μm, as the maximum distance between two samples. This algorithm assigns each cell to a cluster, which is a group of cells, based on the spatial density of cells. The resulting clusters containing at least one pSTAT5^{+} and one secreting cell were defined as cytokine niches, niche score and niche effect were subsequently computed as described in the text. The signaling range was determined using the distances of responding cells to their closest secreting cell inside all niches and calculating the 0.05th largest percentile.